HEAT TRANSFER OF A MULTIPLE HELICAL COIL HEAT EXCHANGER USING A MICROENCAPSULATED PHASE CHANGE MATERIAL SLURRY

A Thesis

by

TRAVIS JOHN GASKILL

Submitted to the Office of Graduate Studies of
Texas A&M University
in partial fulfillment of the requirements for the degree of

MASTER OF SCIENCE

December 2011

Major Subject: Mechanical Engineering

Heat Transfer of a Multiple Helical Coil Heat Exchanger Using a Microencapsulated Phase Change Material Slurry

HEAT TRANSFER OF A MULTIPLE HELICAL COIL HEAT EXCHANGER USINGA MICROENCAPSULATED PHASE CHANGE MATERIAL SLURRY

A Thesis

by

TRAVIS JOHN GASKILL

Submitted to the Office of Graduate Studies of
Texas A&M University
in partial fulfillment of the requirements for the degree of

MASTER OF SCIENCE

Approved by:

Chair of Committee,	Jorge L. Alvarado
Committee Members,	Yassin A. Hassan
	Debjyoti Banerjee
Head of Department,	Jerald Caton

December 2011

Major Subject: Mechanical Engineering

ABSTRACT

Heat Transfer of a Multiple Helical Coil Heat Exchanger Using a Microencapsulated Phase Change Material Slurry.

(December 2011)

Travis John Gaskill, B.S., University of Colorado

Chair of Advisory Committee: Dr. Jorge L. Alvarado

The present study has focused on the use of coil heat exchangers (CHEs) with microencapsulated phase change material (MPCM) slurries to understand if CHEs can yield greater rates of heat transfer. An experimental study was conducted using a counterflow CHE consisting of 3 helical coils. Two separate tests were conducted, one where water was used as heat transfer fluid (HTF) on the coil and shell sides, respectively; while the second one made use of MPCM slurry and water on the coil and shell sides, respectively. The NTU-effectiveness relationship of the CHE when MPCM fluid is used approaches that of a heat exchanger with a heat capacity ratio of zero. The heat transfer results have shown that when using a MPCM slurry, an increase in heat transfer rate can be obtained when compared to heat transfer results obtained using straight heat transfer sections. It has been concluded that the increased specific heat of the slurry as well as the fluid dynamics in helical coil pipes are the main contributors to the increased heat transfer.

To all of my friends and family who have helped guide me to this apogee, I would not be here without you.

ACKNOWLEDGEMENTS

I would like to thank Dr. Jorge Alvarado as the chair of my advisory committee. Thank you for taking the time out of your extremely busy life to allow me to do my research under your guidance. I thoroughly enjoyed the experience working with you. I would like to thank Dr. Wilson Terrell Jr. of Trinity University for spending his time and traveling to College Station to help Dr. Alvarado and me on this research. I would like to thank Dr. Yassin Hassan and Dr. Debjyoti Banerjee for their support and their presence on my advisory committee. I would like to thank Dr. Hessam Taherian for his cooperation during this project as well as for the design and manufacturing of the present heat exchanger. I would like to thank Kalpana Tumuluri for her help in the data reduction of the experiment.

I would like to thank my mother, Sharon Gaskill, for her unending support and love through my childhood and adulthood. Your life guidance is unmatched by any other and I couldn't have asked for anyone better. I would like to thank my father, Jack Gaskill, for his guidance in helping me make some of the best choices of my life. You have taught me the steps of how to live a successful and fulfilling life and I can only hope to continue to achieve them to the extent that you have. I love you both so much; this is for you as much as it is for me. I would also like to thank Jim and Jennifer Misko. You have both been inspirations and friends throughout my life and helped me persevere to achieve something that was once so far away. I would like to thank my cat, Flotsam, for being there with me for the two years of his life. Thank you all so much.

TABLE OF CONTENTS

Page

LIST OF FIGURES

Page

LIST OF TABLES

Page

NOMENCLATURE

A	Area, m^2
A_c	Cross-sectional area, m^2
b	Coil pitch, m
C	Heat capacity, W/°C
c_m	Mass fraction of MPCMs
C_p	Specific heat, J/kg·°C
C_r	Heat capacity ratio, C_{min}/C_{max}
d	Coil tube diameter, m
D	Curvature diameter, m
D_h	Hydraulic diameter, m
De	Dean number
f	Friction factor, Pa·s
f_s	Friction factor of straight pipe, Pa·s
F	Volume fraction
h	Convective heat transfer coefficient, W/m^2·°C
He	Helical number
k	Thermal conductivity, W/m·°C
L	Length of coil, m
$\dot{m}$	Mass flowrate, kg/s

n	Number of carbon atoms minus one
NTU	Number of transfer units
Nu	Nusselt number
Pr	Prandtl number
P_w	Wetted perimeter, m
q	Total heat load, W
Ste	Stefan number
T	Fluid temperature, °C
U	Overall heat transfer coefficient, $W/m^{2}\cdot°C$
V	Velocity, m/s
$\dot{V}$	Volumetric flowrate, m^3/s
w	Heat transfer contribution fraction of each coil

Greek Letters

α	Thermal diffusivity, m^2/s
γ	Dimensionless pitch, b/πD
δ	Curvature ratio, d/D
ε	Effectiveness
λ	Latent heat of fusion, J/kg
μ	Dynamic viscosity, kg/s
ν	Kinematic viscosity, m^2/s
ρ	Density, kg/m^3

Φ	Correction factor, Pr_{bulk}/Pr_{wall}

Subscripts

c	Cold fluid
h	Hot fluid
i	Inside of coiled tube
lm	Log mean temperature difference
m	Mass
o	Outside of coiled tube
t	Tube
s	Shell
w	Water
MPCM	Microencapsulated Phase Change Material

1. INTRODUCTION: THESIS OBJECTIVES

The objective of this thesis is to understand the area of heat transfer research pertaining to coil heat exchanger performance when microencapsulated phase change material (MPCM) slurries are used a heat transfer fluid (HTF). An in depth survey of the literature pertaining to both coil heat exchangers and MPCMs has been conducted in an effort to understand the effect of using MPCMs as HTFs in different heat exchangers. Unfortunately, little has been published in this area. This review will cover the basic understanding of heat exchangers under laminar and turbulent flow as well as a more in depth review of helical coil heat exchangers and their flow and heat transfer characteristics. Previous research in the field of MPCM's is also presented to help understand the effects of their thermal properties including density, viscosity, thermal conductivity, and specific heat on heat transfer performance. A detailed description of the present experimental setup is given and includes physical dimensions as well as operating parameters. Steps taken during the data reduction process is shown in order to understand and analyze the results. Experimental results for the cases of water in the shell with water in the coils, and water in the shell with MPCM slurry in the coils are compared to each other as well as to heat transfer correlations from previous studies. Heat exchanger effectiveness calculations and results are also presented. Using these analyses, conclusions can be made on the effects of using MPCM slurry in helical coil heat exchangers. Finally, future research direction is proposed based upon the present results.

This thesis follows the style of the Journal of Heat Transfer.

2. LITERATURE REVIEW

The present research pertains to both the field of coil heat exchangers (CHE) and MPCMs, and as such, a separate review of the past research in both fields is presented. The review covers the basics of each field as well as any pertinent past research. A preliminary overview of straight tube heat exchangers is conducted to become familiar with the elementary principles.

2.1 Straight Tube Heat Exchangers

There has been a number of research studies conducted on heat exchangers in the past century to quantify the parameters affecting their heat transfer characteristics. A heat exchanger uses two fluids with a temperature difference to transfer heat from one to another, most commonly through a solid interface. Heat exchangers come in a variety of shapes and sizes and are used in almost every industry imaginable including automotive, oil, semiconductor, HVAC, and alternative energy. One of the most common heat exchangers in use is the concentric tube counterflow heat exchanger involving a straight pipe and a straight pipe shell with the inner and outer fluids flowing in the opposite direction as seen in Figure 1.

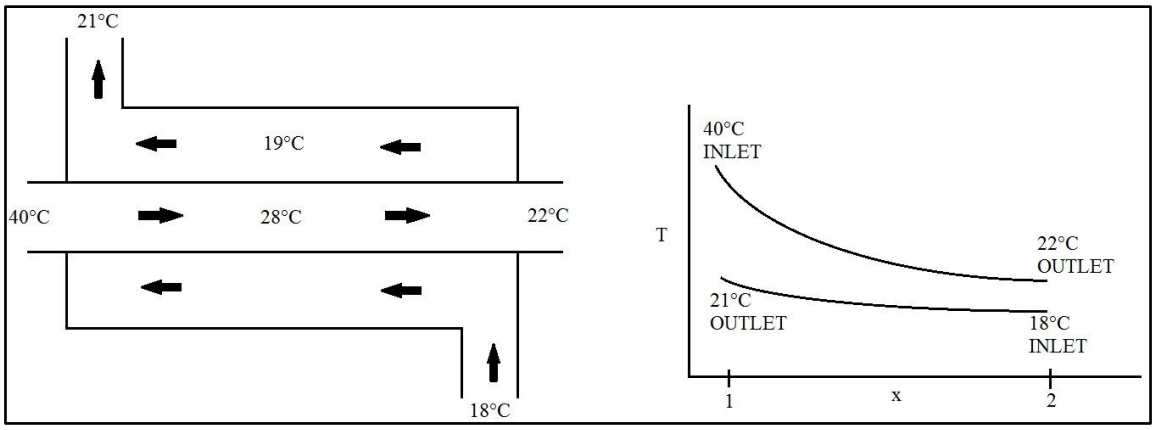

Figure 1: Counterflow heat exchanger and its temperature distribution along its axis

The study of concentric tube heat exchanger can be broken down into fluid flow and heat transfer characteristics, with flow of one fluid through straight pipe and flow of another fluid through an annulus. Straight tube flow has been studied experimentally since the late 19th century by Reynolds, Chilton and Colburn, Dittus and Boelter, Petukhov, Sieder and Tate, as well as Gnielinski [1]. Dittus-Boelter and Gnielinski have developed well-known heat transfer correlations for fully developed turbulent flow in a circular pipe, as seen in Equation (1) and (2) respectively [1].

$$Nu_d = 0.023\, Re_d^{\frac{4}{5}} Pr^n \tag{1}$$

$$n = 0.4 \text{ for heating, } 0.3 \text{ for cooling}$$

$$0.7 \leq Pr \leq 160$$
$$Re_d \gtrsim 10{,}000$$
$$L/d \gtrsim 10$$

$$Nu_d = \frac{(f/8)(Re_d - 1000)Pr}{1 + 12.7(f/8)^{1/2}(Pr^{2/3} - 1)} \tag{2}$$

$$0.5 < Pr < 2000$$
$$3000 < Re_d < 5 \times 10^6$$

From these correlations, heat transfer through a straight pipe is seen to be a function of Reynolds number, Prandtl number, and friction factor as defined below in Equations (3) and (4)[1].

$$Re_d = \frac{\rho V d}{\mu} \tag{3}$$

$$\mathrm{Pr} = \frac{v}{\alpha} = \frac{C_p \mu}{k} \tag{4}$$

$$D_h = \frac{4A_c}{P_w} \tag{5}$$

Such correlations can be used for pipes with non-circular cross sections such as square ducts and annular pipes by replacing the inner diameter, d, with hydraulic diameter, D_h, as defined in Equation (5), where A_c is the cross-sectional area and P_W is the wetted perimeter.

2.2 Helical Coil Heat Exchangers

In an effort to provide the same amount of heat transfer as a straight tube heat exchanger in a smaller space, engineers replace the straight inner pipe with a helical coil. This allows for more heat transfer surface area in a smaller length shell, but increases the pressure drop across the heat exchanger. Helical coil heat exchangers have a more complex flow pattern due to the geometrical configuration of helical coils, which also impart additional centrifugal force on the inner coil flow and increasing the pressure drop on the shell side.

To fully understand the variables effecting helical coil heat transfer, the Dean number is often used and is defined as seen in Equation (6). The Dean number represents the ratio of the viscous force acting on a fluid flowing in a curved pipe to the centrifugal force. The Dean number will never be larger than the Reynolds number for the same flow. As the Dean number approaches that of the Reynolds number, the effects of centrifugal force dominate the flow. This phenomenon and its effects on heat transfer have been studied extensively.

$$De = \frac{\rho V d}{\mu}\sqrt{\frac{d}{D}} = Re\sqrt{\frac{d}{D}} \tag{6}$$

In 1963, Seban and McLaughlin [2] studied heat transfer through a helical coil using two different curvature diameter ratios, d/D, of 0.0588 and 0.0096. The curvature diameter ratio is defined as the ratio of the inner diameter of the pipe, d, to the curvature diameter of the helix, D. The flow was varied from laminar to turbulent for a range of $12 < Re < 65{,}000$. Heat was applied to the coil through the use of an AC current along the length of the stainless steel coil. This provided for an almost constant heat flux boundary condition and is known as Joule Heating. The experimental set up consisted of multiple coils with multiple thermocouples on each coil. It was noted that even though circumferential conduction of heat was neglected, due to the nature

of the flow in a helical coil, the heat transfer coefficients at the inside and outside halves of the pipe were substantially different in the laminar flow regime. Pressure taps were also included on each end of the coil bank. The local heat transfer coefficients for laminar flow were found to be consistently larger on the outer half (peripherally) than on the inner half. For all cases, a larger heat transfer coefficient was seen relative to a straight tube. There was also evidence to support a shorter entry length region, resulting in a shorter distance before asymptotic heat transfer values were reached. The asymptotic value was shown to be a function of $RePr^{0.3}$, and was not constant as is seen in straight tube flow. In the laminar region, there was no evidence to support a dependency on the curvature diameter ratio, as the heat transfer coefficients for the large and small coils were similar. An empirical best fit of the data was given in the form of Equation (7) based upon the asymptotic heat transfer coefficients, where *A* and *B* are found based upon a curve fit.

$$Nu = A \cdot Re^{B} Pr^{1/3} \tag{7}$$

$$\frac{f}{8} = \frac{Nu}{Re \cdot Pr} Pr^{2/3} \tag{8}$$

Due to the similarity of this equation to the Dittus-Boelter correlation, it was assumed that these heat transfer coefficients could be related to the friction factor in a way similar to the Chilton-Colburn analogy as seen in Equation (8). This analogy relates friction factor to Nusselt number for fully developed turbulent flow in a smooth circular tube [1]. Seban and McLaughlin proposed a Nusselt number correlation in Equation (9), where A is based upon a curve fit. In this case, $A = 0.13$ produced the best fit for both curvature diameter ratios. It was noted that this correlation should be applicable to any helical coils under the range of conditions where $12 < Re < 5{,}600$, $100 < Pr < 657$, and $17 < D/d < 104$ under constant heat flux. Under the studied turbulent flow range $6000 < Re < 65{,}600$ there was still a visible difference between the heat transfer coefficients of the inner and outer halves of the coil but to a lesser extent under turbulent flow. In accordance with straight pipe flow, the heat transfer coefficients were plotted versus $RePr^{0.4}$. The Prandtl number is to the 0.4 power due to the flow undergoing heating. It was

shown that the average peripheral heat transfer coefficient deviated by less than 10% from the proposed correlation in Equation (10) for the large coil, where the friction factor in this case was calculated from an empirical correlation also presented in the study.

$$Nu = A\left[\frac{f}{8}Re^2Pr\right]^{1/3} \tag{9}$$

$$Nu = \frac{f}{8}RePr^{0.4} \tag{10}$$

In 1971, Dravid [3] conducted a numerical and experimental study on heat transfer through coils. The research was restricted to the laminar regime but for *De* > 100. The numerical results were based upon helical coils with small curvature diameter ratios and fully developed velocity fields. Based upon previous research, the predicted flow field based upon Dean number can be seen in Figure 2. The numerical results showed that due to the complex flow field, large cyclical oscillations in axial wall temperature occur with the oscillations being damped at larger axial distances.

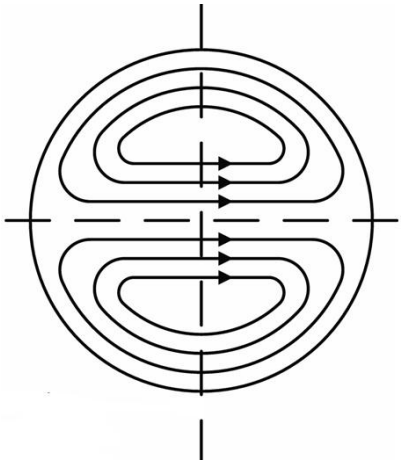

Figure 2: Secondary flow field in helical coiled tubes [4]

Their experimental setup consisted of thick copper tubing helically wrapped in a Teflon coated Nichrome wire. This was then formed into a helix with a curvature diameter of 137 mm (5.4 in).

creating an overall curvature diameter ratio, $d/D = 0.0536$. It should be noted here that many studies refer ambiguously to curvature diameter ratio, and unless otherwise noted, it should be thought of as d/D. Water was used as the working fluid. The experimental results matched very well with the numerical results, both showing damped oscillatory motion. The short entry length region relative to a straight tube was also seen in the experiment. Based upon the asymptotic Nusselt numbers found experimentally, the correlation in Equation (11) is proposed for $50 < De < 2000$ and $5 < Pr < 175$ with a standard deviation of 6%.

$$Nu = \left[0.76 + 0.65\sqrt{De}\right]Pr^{0.175} \tag{11}$$

In 1974, Kalb and Seader [5] produced a numerical study on helical coiled tubes for Dean numbers up to 1200. The boundary condition was chosen to be constant axial surface temperature, as at the time it was the least studied condition, as well as it having more applicability to real world scenarios. Based upon their analysis, the fully developed temperature field was shown to change markedly with increasing Prandtl number. It was also shown that the thermal boundary condition plays a role in fully developed temperature profiles, with a uniform wall temperature boundary condition contributing to a wider range of temperatures from the wall to the core of the flow field. It was also shown that for middle range Prandtl numbers of 0.7 to 5, the boundary condition of uniform wall temperature provides for a Nusselt number with a smaller dependence on Prandtl number when compared with uniform axial heat flux boundary condition. Kalb and Seader proposed Equation (12) as a helical coil heat transfer correlation, valid for $0.7 < Pr < 5$, $80 < De < 1200$ and $0.01 < d/D < 0.1$.

$$Nu = 0.836De^{0.5}Pr^{0.1} \tag{12}$$

In 1978, Janssen and Hoogendoorn [6] produced a numerical and experimental study that was focused on Prandtl numbers from 10 to 500. The experimental setup consisted of helically coiled stainless steel tubes and Joule Heating was used to produce an axially uniform heat flux boundary condition. The experiment also considered a constant surface temperature boundary condition by placing the coil in a shell with condensed steam. The numerical results showed the same damped cyclical nature of the Nusselt number as seen from Dravid [3]. It was also seen

that for $De < 20$, the asymptotic Nusselt number was correlated with De^2Pr. The proposed correlation as seen in Equation (13) is valid for $De < 20$ and $(De^2Pr)^{1/2} > 1\ x\ 10^2$. The experimental results showed that for $De > 20$, the Nusselt number had little dependence on d/D and was proportional to $Pr^{1/6}$, which is unlike the previous studies. The results also showed little difference between the Nusselt numbers from the different boundary conditions, which was mostly assumed to be due to the low temperature dependent viscosity of the fluid in the experiments. Janssen and Hoogendoorn also proposed the correlation seen in Equation (14), valid for $1\ x\ 10^2 < De < 8.3\ x\ 10^2$.

$$Nu = 1.7(De^2Pr)^{1/6} \tag{13}$$

$$Nu = 0.7Re^{0.43}Pr^{1/6}(d/D)^{0.07} \tag{14}$$

In 1981, Manlapaz and Churchill [7] conducted a review of all of the previous experimental and numerical results involving heat transfer in coiled tubes. Their goal was to produce a general correlation for all the different regimes covering $0 < De < 2000$ and $0 < Pr < 1600$. There were also efforts to include the effects of finite pitch into the correlation. This was done by replacing the Dean number with the Helical number as seen in Equation (15).

$$He = De/[1 + (b/\pi D)^2]^{1/2} \tag{15}$$

It was shown that for values of $b/(D/2)$ less than unity, the effects of pitch, could be neglected. General correlations were produced for both constant axial heat flux and constant surface temperature boundary conditions. It was noted that the experimental results used to calculate these correlations did not go beyond a Helical number of 2000 and that any values predicted past this value were purely speculative. The correlations for constant heat flux and constant surface temperature boundary conditions are presented in Equations (16) and (17), respectively.

$$Nu = \left[\left(\frac{48}{11} + \frac{51/11}{\left(1 + \frac{1342}{PrHe^2}\right)^2}\right)^3 + 1.816\left(\frac{He}{1 + \frac{1.15}{Pr}}\right)^{3/2}\right]^{1/3} \tag{16}$$

$$Nu = \left[\left(3.657 + \frac{4.343}{\left(1 + \frac{957}{PrHe^2}\right)^2}\right)^3 + 1.158\left(\frac{He}{1 + \frac{0.477}{Pr}}\right)^{3/2}\right]^{1/3} \tag{17}$$

In 1989, Prasad et al. [8] conducted an experiment on a coiled tube in a shell, which was one of the first recent experiments on a helically coiled tube in shell heat exchanger. The experimental setup consisted of copper helical coils with diameter ratios *D/d* of 17.24 and 34.90 for two separate tests. The coils were placed in a large shell. The working fluids used were hot water and air for the coil and shell sides, respectively. The experiments measured both pressure drop and temperature along the coil and shell. The experiments were conducted throughout the laminar and turbulent regime for 1780 < *Re* < 59,500. The transition from laminar to turbulent regime was determined by the critical Reynolds correlation developed by Ito [9] and used by Seban and McLaughlin [2], as seen in Equation (18). The correlation proposed for the laminar regime is of the same form as Seban and McLaughlin (1963) as seen in Equation (9), but in this case A = 0.25 for 200 < *De* < 500. A new correlation for the turbulent regime was not proposed, but rather it is said to correlate well with Equation (10) from Seban and McLaughlin (1963). Prasad also proposed shell side correlations similar to the form of the Dittus-Boelter correlation for flow in a circular annulus as seen in Equation (19), where C is a function of *D/d* ratio. The variable, *C*, was found to be 0.057 and 0.110 for *D/d* = 17.24 and 34.90, respectively. Equation (19) is valid for 30,000 < Re_{Dh} < 200,000.

$$Re_{Cr} = 2\,x\,10^4\left(\frac{d}{D}\right)^{0.32} \tag{18}$$

$$Nu_s = C \cdot {Re_{Dh}}^{0.8} \tag{19}$$

In 1997, Yildiz et al. [10] conducted an experimental study on a helical tube in a shell heat exchanger containing inside springs. The springs were placed inside the helical tube as a way to passively increase the heat transfer inside the loop. The experimental setup consisted of 5 mm helical pipes with a curvature diameter of 75 mm. The shell was well insulated and air and water were used as the working fluids in the coil and shell sides, respectively. It was not stated whether the air was undergoing heating or cooling but as the data was compared to the Dittus-Boelter correlation seen in Equation (20), we can assume it was undergoing heating. The information we are interested in for this present research is the results of the experiments without springs. The correlation, seen in Equation (21), was presented in the same form as in Equation (20), valid for $1265 < De < 2850$ and $Pr = 0.7$. As for the results with the introduction of the spring in the coil, an increase in heat transfer effectiveness of up to 30% is seen in the heat exchanger while the pressure drop also increases up to 10 times that of the empty tube flow.

$$Nu = 0.023 Re^{0.8} Pr^{0.4} \tag{20}$$

$$Nu = 0.0551 De^{0.864} Pr^{0.4} \tag{21}$$

In 1998, Guo et al. [11] experimentally studied the effects of pulsatile flow on heat transfer in helically coiled tubes. The experiment was conducted using two-phase steam water as the working fluid. The experiment had a total of 102 thermocouples on the outside of the tube, varied axially as well as peripherally. This provided a very detailed description of the temperature field. Part of the experiment was conducted under steady single-phase flow. The results for steady flow indicated that for $6000 < Re < 60{,}000$, the Seban MchLaughlin (1963) correlation seen in Equation (10) accurately described the system. For larger Reynolds numbers, the enhancing effect of the secondary flow due to the helical coil became less significant and once again fell towards the predicted values by the Dittus-Boelter correlation seen in Equation (1). Guo et al. proposed the correlation as seen in Equation (22) for $6000 < Re < 180{,}000$. It was also shown that due to the orientation of the coil, the positions of upward flow relative to gravity gave an increase in heat transfer. It was also shown, in congruence to previous experiments, that the heat transfer coefficient on the outer half of the coil is consistently larger than the heat transfer on the inner half.

$$Nu = 0.328Re^{0.58}Pr^{0.4} \tag{22}$$

A 2005 study by T. J. Rennie [12] focused on an experimental study of a helical pipe in pipe heat exchanger. The idea was to reduce the possible zones of dead or no flow in a coil in shell heat exchanger by creating 2 helical pipes, one inside of another. The experimental setup consisted of only 1 turn of a coil with zero pitch so the applicability of the results is somewhat questionable. A large and a small inner coil were tested with the same outer annulus. Regardless, the only measurements taken were of the inlet and outlet temperatures of the inner tube and outer annulus. This was done to not affect the flow field. In order to calculate inner and outer heat transfer coefficients, the Wilson Plot method was used. This method uses the inlet and outlet temperatures and the calculated overall heat transfer coefficient to calculate inner and outer heat transfer coefficients. There is also the assumption that by keeping the mass flow rate of the inner tube constant, it can be assumed that the inner heat transfer coefficient is constant. This method is described in detail by Fernandez-Seara [13]. The results for the inner heat transfer coefficient were similar to that of Dravid [3], but due to the increased variability in the results of the smaller inner coil, the Wilson Plot method did not work as well. The results also showed that operating in parallel or counterflow configuration, the overall heat transfer coefficient did not change appreciably.

A 2006 experimental and numerical study by V. Kumar et al. [14] was conducted on a tube in tube helical heat exchanger. Unlike Rennie [12], the setup had 4 coil turns, providing a larger length for the flow to develop. Hot and cold water were used as the working fluids for the inner coil and outer annulus, respectively. The heat exchanger was operated in the counterflow configuration. The inner and outer tube diameters were 25.4 and 50.8 mm, respectively. The outer annulus contained baffles to hold up the inner coil as well as induce more turbulence. Like Rennie [12], the heat transfer coefficients were calculated using the Wilson Plot method. A numerical analysis was also conducted using the same system design and boundary conditions using FLUENT 6.1. The inner Nusselt number experimental results were compared with the numerical results and were seen to deviate by less than 4%. This provides at least some evidence supporting the viability of the Wilson Plot method for future researchers. The values of the inner Nusselt number reported are slightly higher than the correlations of Kalb and Seader [5] and Manlapaz and Churchill [7] but follow the same trend. The discrepancy was most likely due to

the change in boundary conditions. The outer Nusselt number experimental and numerical results deviate 8-10% from each other, and are seen to be 2-3 times higher than straight tube flow.

In 2007, Naphon [15] conducted a study on a complex heat exchanger involving two helical coil banks with fins attached to the coils, inside of a sectioned shell. The heat exchanger was operated in the counter flow configuration. Hot water and cold water were used for the coil and shell sides, respectively. Though no results were presented on inner or outer heat transfer coefficients, results were given relating the heat exchanger effectiveness versus shell and coil flowrates. For low hot water mass flowrates, the heat exchanger effectiveness was seen to increase with increasing coil hot water inlet temperature. At higher hot water flowrates, the effectiveness converges onto a single value, regardless of hot water inlet temperature. The highest effectiveness is seen with the largest shell side flowrate and the lowest coil side flowrate, and the lowest effectiveness is seen when the inverse situation occurs.

A 2008 study by M.R. Salimpour [16] presents the first known analysis of the effects of temperature dependent fluid properties on a shell and helical coil heat exchanger. The fluid used in the coils was Behran Hararat oil and had temperature dependent properties correlated to equations from a previous study to within an accuracy of 1%. The temperatures and pressure drops for both the inlet and outlet of the shell and coil were measured and the properties were evaluated at their mean and mean caloric temperatures, respectively. The tests were conducted at three different oil temperatures in order to study the effect of fluid temperature. The shell side heat transfer coefficient was calculated from a correlation developed in a previous study by Salimpour [17] and from this and the experimental data, inner heat transfer coefficients were calculated. The inner Nusselt numbers presented are higher than and largely deviate from the values predicted by Dravid [3]. This could be due to both the different boundary conditions and the effect of temperature dependent properties. By testing three different coils, it was shown that reducing coil pitch increased the inner heat transfer coefficient due to the increased effect of the secondary flow. Salimpour proposes the correlation seen in Equation (23) for the range $35 < De < 410$, $0.058 < \gamma < 0.095$, $160 < Pr < 325$, $0.113 < \delta < 0.157$, and $0.34 < \Phi < 0.60$.

$$Nu_i = 0.554 De^{0.496} \gamma^{-0.388} Pr^{0.151} \Phi^{0.153} \tag{23}$$

In 2009, Kharat et al. [18] conducted a numerical and experimental study of a working thermic fluid heater. The heat exchanger under study consisted of two helical coil tube banks with pitch equal to the coil diameter, making a concentric coil annulus. The study focused on the shell side heat transfer, and as to whether shell side heat transfer should be predicted based upon the existing formats for tube banks or for flow through a concentric annulus. Results concluded that a correlation based upon a tube bank greatly over predicted the shell side Nusselt number. A correlation based upon a concentric annulus was shown to under predict the experimental results by an average of 29%. The numerical study allowed for certain variables to be looked at including coil tube diameter as well as coil annulus gap based upon the outer edge of the coils. A correlation was proposed including a new dimensionless variable known as Gap ratio as seen in Equation (24). The new correlation proposed is seen in Equation (25), valid for 20,000 < *Re* < 150,000 and a coil gap/tube diameter ratio from 0.55 to 2.25.

$$Gap\ ratio = (D_o - D_i)/d \tag{24}$$

$$Nu_o = 0.0265 Re^{0.835} Pr^{0.3} (Gap\ ratio)^{-0.097} \tag{25}$$

In 2009, M.R. Salimpour [19] conducted an experimental study on a shell and helical coil heat exchanger using cold and hot water for the shell and coil sides, respectively. There were three different coils tested, varying in pipe diameter and pitch. The tube and shell side flow rates were measured as well as the inlet and outlet temperatures for both. The fluid properties were evaluated at their mean temperature. The outer heat transfer coefficients were calculated using the Wilson Plot method. A total of 75 outer heat transfer coefficients were calculated based upon five different shell side flow rates, leading to a total of 15 calculated inner heat transfer coefficients. The results indicate a good agreement with [7] when taking into account the constant surface temperature boundary condition correlation proposed by Manlapaz and Churchhill [7] seen in Equation (17) for *De* < 3000, while it over predicts for values higher than this. It was also seen, as in [16], that the inner Nusselt number increases with decreasing coil pitch. The proposed correlation for inner Nusselt number can be seen in Equation (26) and is valid for 1000 < *De* < 5000. The same variables were chosen to represent the shell side heat

transfer coefficient except replacing Dean for Reynolds number, with the correlation as seen in Equation (27) for $60 < Re_o < 500$. It should be noted that the shell side hydraulic diameter, D_h, is calculated using Equation (28).

$$Nu_i = 0.152De^{0.431}Pr^{1.06}\gamma^{-0.277} \tag{26}$$

$$Nu_o = 19.64{Re_o}^{0.513}Pr^{0.129}\gamma^{0.938} \tag{27}$$

$$D_h = \frac{{D_s}^2 - \pi D_c {d_o}^2 \gamma^{-1}}{D_s + \pi D_c d_o \gamma^{-1}} \tag{28}$$

A 2009 experimental study by Mandal and Nigam [20] uses the same exact tube in tube helical heat exchanger as used by Kumar [14]. In this case, the experiments were conducted using water and compressed air for the annulus and inner coil respectively. The inner coil flow was tested between $14{,}000 < Re < 86{,}000$. The present results for the inner coil Nusselt number were found to be larger than predicted values from previous correlations. This is most likely due to the use of compressed air as a working fluid or the counterflow heat exchanger boundary condition present in the experiment. Regardless, a new empirical correlation was postulated as seen in Equation (29). For reference, the outer annular-coiled tube is also seen to outperform previous results and correlations. This was possibly due to the use of semicircular baffles in the annular region to induce turbulence, thus increasing heat transfer.

$$Nu_c = 0.55De^{0.637}Pr^{0.4} \tag{29}$$

In 2010, H. Mirgolbabaei et al. [21] conducted an experimental and numerical study on a helical coil in an annulus heat exchanger. The experiment consisted of a numerical study with seven test coils of different pitch and tube diameter in an annular shell. The numerical data was then compared to an experimental result involving one test coil with an outer tube diameter and coil pitch of 9.52 and 16.57 mm, respectively. The temperatures and flowrates were measured at the inlet and outlet of the shell and coil. Cold and hot water were used as the shell and coil side working fluids, respectively. The study focused on specifically the shell side heat transfer

coefficient. It was shown that there are multiple ranges of coil pitch that affect the heat transfer coefficient. For a dimensionless coil pitch of 1.8, decreasing or increasing the pitch to 1.5 or 2 increases the shell side heat transfer coefficient. Increasing the tube diameter was shown to decrease the heat transfer coefficient under the same amount of heat flux for the same coil pitch. Based upon a dimensional analysis of several different possible variables for characteristic length, a normalized length was chosen to provide the strongest correlated data, producing the correlation seen in Equation (30), valid for 8.1 x 10^6 < Ra_{Ln} < 2.2 x 10^8 and 40 < Re_{Ln} < 205.

$$Nu_{Ln} = 0.073\left(\frac{D_t}{D_c}\right)^{-0.769} Re_{Ln}{}^{0.005} Pr_{Ln}{}^{0.15} Ra_{Ln}{}^{0.231} \tag{30}$$

A 2010 study by N. Ghorbani et al. [22] focused on the shell side heat transfer of a shell and helical coil heat exchanger. The working fluids were cold and hot water for the shell and coil sides, respectively. The experiment is studied in the mode of mixed convection, taking into account the effects of Raleigh number as well as Reynolds number. The tests were conducted using both laminar and turbulent flow inside the coil. Though some of the analysis is questionable, Equation (31) was proposed for the shell side Nusselt number for 2.5 x 10^7 < Ra_{Dhx} < 3.5 x 10^8 and 150 < Re_{Dhx} < 1200. In this case, hydraulic diameter is defined by Equation (32). N. Ghorbani et al. [23] presented this same experimental data in another 2010 paper focusing on the heat exchanger effectiveness. It was shown that the effectiveness-NTU relationship closest resembled that of a counterflow concentric tube heat exchanger and was the suggested relationship to use in further ε-NTU calculations, as seen in Equation (33).

$$Nu_{Dhx} = 0.0013 Ra_{Dhx}{}^{0.5128} Re_{Dhx}{}^{0.2} Pr_s{}^{0.3} \tag{31}$$

$$Dhx = \frac{4A_c H}{P_w} \tag{32}$$

$$\varepsilon = \frac{1 - exp[-NTU(1 - C_r)]}{1 - C_r \cdot exp[-NTU(1 - C_r)]} \tag{33}$$

2.3 Microencapsulated Phase Change Material (MPCM)

In the past 25 years, engineers and researchers have begun to introduce new materials and fluids into heat exchangers in hopes of increasing heat transfer performance. Materials that change phases within the operational temperatures of the heat exchangers were studied in order to utilize the added heat capacity from the latent heat of melting of the material. When introduced into the heat exchanger fluid, the new material is shown to increase heat capacity with the same or less temperature difference as before. However, without somehow avoiding the separation or precipitation of the phase change material from the working fluid during the solidification process, the phase change material tended to agglomerate and create obstructions in heat exchangers. To prevent this, microencapsulated phase change materials (MPCMs) were introduced. The idea behind this was to prevent agglomeration while still obtaining increased specific heat of the working fluid during the phase change process. A considerable number of studies have been conducted in the last 15 years in order to better understand the processes by which the introduction of MPCMs affects heat transfer.

In 1999, Y. Yamagishi [24] conducted an in-depth study on the flow and heat transfer characteristics of an MPCM slurry under constant heat flux. The phase change material (PCM) used was Octadecane, which has a latent heat of 223 kJ/kg. The particles had an average diameter of 6.3 μm. It was assumed the average capsule thickness was 0.1 μm. The particles were mixed with water at five different varying volume fractions from 0.07 to 0.30. As shown in previous study, microencapsulating a PCM causes some degree of supercooling, the difference in temperature between the melting and solidification temperature. The solidification temperature of MPCM's will be somewhat lower than the melting temperature, and is detrimental to the heat transfer process. The amount of supercooling was reduced from 13 K to 5 K by the introduction of a dispersing agent into the phase change material before the encapsulisation process. Heat transfer tests with MPCM/water were compared to tests with water using a well calibrated heat transfer loop. The MPCM slurry was tested in the loop with zero heat flux to provide insight on the rheological properties of the fluid. The results show the MPCM slurry acts as a Newtonian fluid, with a transition from laminar to turbulent regime around a Reynolds number of 2300, which is normal for circular pipe flow. It was also seen the pressure drop for increasing MPCM volume fraction increased for the same mean flow velocity due to the increased slurry viscosity.

From this information it was found that there is a nonlinear relationship on viscosity versus particle volume fraction. In almost all the cases, the temperature of the flow has three distinct regions similar to the Figure 3. Regions I and III corresponded to a temperature increase due to the sensible heat of the slurry, while Region II begins at the point of MPCM melting temperature. This temperature theoretically remains constant until all the particles have melted where it once again begins to increase in temperature due to the thermal energy gain from sensible heat. With a lower heat flux, Region II becomes larger, not allowing the particles to completely melt before the end of the test section. The experimental results slightly deviate from the calculated results of Figure 3 due to the supercooling phenomenon as well as the finite melting rates of the particles.

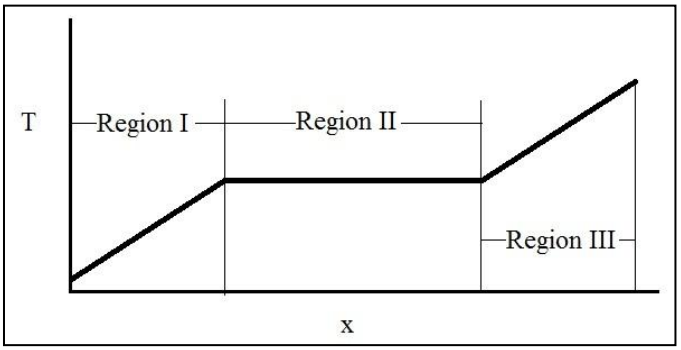

Figure 3: Temperature vs. Axial distance for a MPCM slurry under constant heat flux

When comparing the local heat transfer coefficients of water versus MPCM slurry for the same flowrate, at the beginning and the end of the test section the MPCM is seen to have a markedly lower heat transfer coefficient being due to the increased slurry viscosity. In Regions I and II however, an increase in heat transfer coefficient is seen, with a maximum slightly under the heat transfer coefficient of water. The increase in heat transfer coefficient could be caused by the melting of the MPCM particles; thus increasing the effective specific heat of the slurry. After the particles have melted, a drop is seen in the heat transfer coefficient towards what is predicted by heat transfer to a single-phase fluid. The heat transfer coefficient results also showed that for a larger input heat flux, a lower maximum heat transfer coefficient was achieved, which is thought to be caused by the increasing thickness of the thermal boundary layer, causing the particles in the turbulent core to melt before reaching the tube wall [24]. When comparing heat transfer coefficients for different particle volume fractions under the same inlet temperatures, heat flux,

and Reynolds numbers, the larger particle volume fraction resulted in a larger maximum heat transfer coefficient. However for the same flowrate, a lower volume fraction was seen to have a higher local heat transfer coefficient. This was said to be due to the decrease in turbulence (lower Reynolds number) from the increase in the slurry viscosity, where the lower turbulence did not allow as many particles from the core to travel towards the tube wall. What this means is that higher volume particle fractions will not always result in a higher heat transfer coefficient, as there are competing effects between higher slurry viscosity and a higher effective specific heat. At relatively high mass fractions, a laminarization of the flow was seen to occur, drastically decreasing the local heat transfer coefficients. It was postulated that due to the laminar flow, a layer of fully melted particles forms along the tube wall while the core region is filled with solid particles. It was concluded that for the same particle volume fraction, turbulent flow is more effective than laminar flow, even when the slurry undergoes phase change. In light of all the presented results, it was seen that for the same flowrate in the turbulent flow regime, the local heat transfer coefficient of the MPCM slurry was always lower than that of pure water.

In 2002, Hu and Zhang [25] produced a numerical study on laminar heat transfer of MPCMs in a circular pipe under constant heat flux. The study looked at the thermally developing region as well as the fully developed region. Since the variability of specific heat throughout the melting temperature range of the MPCM is not well known, 4 different functions were looked at and were shown to effect the Nusselt number through the thermal entry region but were shown to converge at large axial distances. The fluid was assumed to have a Newtonian behavior up to a volumetric concentration of 0.25. A sensitivity analysis was conducted to study the effects of the Stefan number, degree of subcooling, melting temperature range, particle diameter, and volumetric concentration on the heat transfer enhancement. Since volumetric concentration affects both the effective thermal conductivity as well as the mean heat transfer coefficient, it was seen to have the largest effect on heat transfer. Based upon the results, a low degree of subcooling, a small melting temperature range, and a large particle diameter were seen to benefit heat transfer the most, but individually not as much as volumetric concentration. As with any other single-phase flow, an increase in Reynolds number was shown to increase the Nusselt number.

In 2007, J. L. Alvarado et al. [26] conducted a study on MPCM heat transfer and pressure drop using a set of heat transfer sections under constant heat flux. The study also included analysis of

the MPCM construction and efforts to reduce the effect of supercooling. The PCM used was Tetradecane with an average size of 2-10 μm. Tetradecanol was used as a nucleating agent to reduce supercooling. Viscosity analysis showed behavior reminiscent of a Newtonian fluid up to mass concentrations of 17.7%. The pressure drop results did not indicate any significant increase in pumping power. The apparent specific heat used in heat transfer analysis was calculated as a function of mass fraction. All results were within the Reynolds range of 3900-7500. The same three-region temperature distribution was seen as shown in Figure 3. Under the same flow conditions, an increase in heat capacity of 40% was seen for 7% mass fraction slurry. Under the same conditions, the heat transfer coefficient was seen to vary along the pipe, reaching a maximum near the melting point of the MPCM. Regardless, at the same flow velocities, a lower heat transfer coefficient was seen for the slurry due to reduced momentum transfer.

In 2008, B. Chen et al. [27] studied heat transfer of MPCM slurry under laminar flow through a circular pipe. The pipe was stainless steel and a constant heat flux boundary condition was applied through Joule Heating by using the pipe as a resistance. The PCM used was 1-bromohexadecane with a melting temperature around 15°C. Density and specific heat of the MPCM were calculated based upon the mean of its solid and liquid properties. The thermal conductivity of the particle was calculated by estimating its thermal resistance. The slurry density and specific heat were calculated based upon the mass fraction. In the region of phase change, the specific heat was taken to be a function of the heat of fusion. The slurry thermal conductivity was calculated using Maxwell's relation. The viscosity of the slurry was shown to be Newtonian for all specimens, up to a 15.8% weight fraction. The effective specific heat of the slurry was seen to increase up to 28.1% relative to water during the phase change process. An applicable pump power analysis was performed to determine the decrease in consumption through using MPCM slurry versus water. Due to the higher heat capacity, a decrease of 67.5% in pump work can be seen while removing 750W using the 15.8% weight fraction MPCM slurry. In 2009, R. Zeng et al.[28] used this same experimental data and compared it to a numerical simulation based upon an enthalpy model. It should be noted that in the phase change region, a sine curve was chosen to represent the changing value of specific heat of the slurry. The Nusselt number along the pipe is shown to reach a maximum at the onset of the melting region and a minimum at the end of the melting region, these values being higher and lower than the numerical results for water, respectively. The Stefan number, seen in Equation (34), as well as the phase change temperature range were shown to effect the Nusselt number the most, while the

effects of particle diameter, Reynolds number, and particle concentration were shown to cause smaller effects.

$$Ste = \frac{C_p \cdot \Delta T_{fus}}{\lambda} \tag{34}$$

In 2010, Taherian [29] presented model analysis of the effects of using a blend of MPCMs and nanofluids in water on heat transfer. The idea behind this is to combine the high effective specific heats of MPCM's with the high thermal conductivity of a nanofluid to produce a better heat transfer fluid than would be seen using the individual constituents. In a simulated counter flow concentric tube heat exchanger, the effects of the percentage of MPCM's that undergo phase change as well as the amount of nanofluids present in the blend were analyzed. The effective specific heat was shown to be large for a high phase change percentage combined with a small mass fraction of nanofluids. At higher nanofluid mass fractions, the effective specific heat converges towards a single value, regardless of the percent of phase change.

In 2010, Nakagawa et al. [30] conducted an experimental study using MPCMs through a circular mini pipe. The PCM used was lauric acid with a melting temperature of about 45°C. The average size of the particle was 3.27 μm and the particle mass concentration was varied from 0 to 5%. Flourinated dielectric fluid was used as the working fluid. The specific heat of the slurry is calculated based upon the single-phase properties and the mass fractions of the fluid and particles. The effect of latent heat was taken into account when total heat transport rate was calculated. The results show that with increase in mass concentration produces a decrease in wall temperature rise along the axis. The overall heat transport rate is shown to increase with increasing mass concentration and increasing flowrate. The results for Nusselt number show good correlation with theory when using the dielectric fluid. When using the slurry, the Nusselt number increases towards the end of the test section, with a maximum Nusselt number of around 35 for a mass concentration of 5%. It was assumed that the high Nusselt number values were overestimated due to the assumption of a bulk fluid linear temperature profile along the axis. Because of the melting process, the temperature of the slurry will vary along the length of the tube, and a linear temperature relationship is not accurate.

As the recent studies show, little to nothing has been done in the field of MPCM as HTF in coil heat exchangers (CHE). This study is a first attempt to understand how MCPMs perform in CHE.

3. EXPERIMENTAL STUDY ON HELICAL COIL HEAT EXCHANGER

In an effort to understand the effect of using a coil heat exchanger on MPCM slurries, an experimental setup consisting of a CHE was designed for that purpose. The MPCM slurry consisting of microcapsules containing methyl-stereate as the phase change material was tested in a heat transfer facility consisting of straight sections for heating, and a CHE for cooling. The straight sections were uniformly axially heated to study the effects of turbulence on the heat transfer characteristics of MPCMs. The experimental setup was the basis for the results presented by Tumuluri [31].

3.1 Experimental Setup

The present experiment relies on the data collected in a multiple helical coil counterflow heat exchanger designed by Dr. Hessam Taherian. The experimental set up consisted of a pump and motor for the coil side, a coil side flowmeter, a water chiller with a built in pump for the shell side, and a data acquisition unit.

3.1.1 Helical Coil Heat Exchanger

The multiple helical coil heat exchanger (CHE) can be seen in its experimental setting in Figure 4. The heat exchanger consists of a copper shell, 4 concentric helical coils with a constant pitch of 13.5 mm (0.53 in) and a solid copper center rod. A cross section view of the heat exchanger SolidWorks model can be seen in Figure 5.

Figure 4: Helical coil heat exchanger without insulation [31]

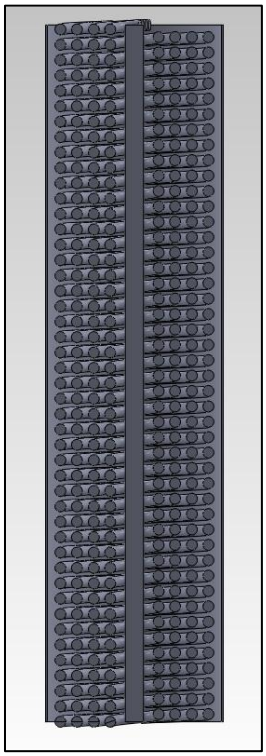

Figure 5:Cut cross section view of heat exchanger Solidworks model

The coil tubing used is 9.5 mm (3/8 in) OD copper tubing with a 6.4 mm (1/4 in) nominal inner diameter. The coils were bent by hand and soldered into place at the inlet and outlets. The shell consisted of a 15.2 cm (6 in) ID copper pipe with a length of 70 cm (24 in). The complete design description for the heat exchanger can be seen in Table 1. During manufacturing, Coil 1 was cracked or pierced and because of this was unable to be used in the experiment. Because the shell caps were brazed on, the coil had to be left inside the heat exchanger, and shut off from the outside during all the experiments. The entire shell was covered in thick foam insulation to prevent external heat loss.

Table 1: Design summary of helical coil heat exchanger

Part	Diameter (cm)	Length (m)	Outer Surface Coil Area (cm^2)	Inner Surface Coil Area (cm^2)
Shell	15.2	0.61	-	-
Coil 1	13.0	17.43	52.2	34.8
Coil 2	10.0	13.53	40.5	27.0
Coil 3	7.1	9.66	28.9	19.3
Coil 4	4.2	5.76	17.2	11.5
Total	-	-	138.8	92.5

3.1.2 Pump

The pump used in the experiment for the MPCM slurry was the same pump that was used in the upstream experiment, as it was one continuous loop. The pump was a Moyno® 500 progressive cavity pump, 300 series. The pump is designed in such a way as to minimize the amount of shearing action on the MPCM particles throughout the tests, which could cause breakage. The style of pump can be seen in Figure 6. The pump is capable of flowrates up to 15 GPM, pressures up to 150 PSI, and fluid temperatures up to 210°F [31].

3.1.3 Pump Motor

Since the progressive cavity pump itself does not have a motor, a 0.746 kW (1 HP) motor was purchased from Century Motors to operate the pump. It operates at 1200 rpm and has a service factor of 1.15. The motor speed was varied by a Grainger adjustable frequency drive using a 1-phase input power supply with 200-240 V [31].

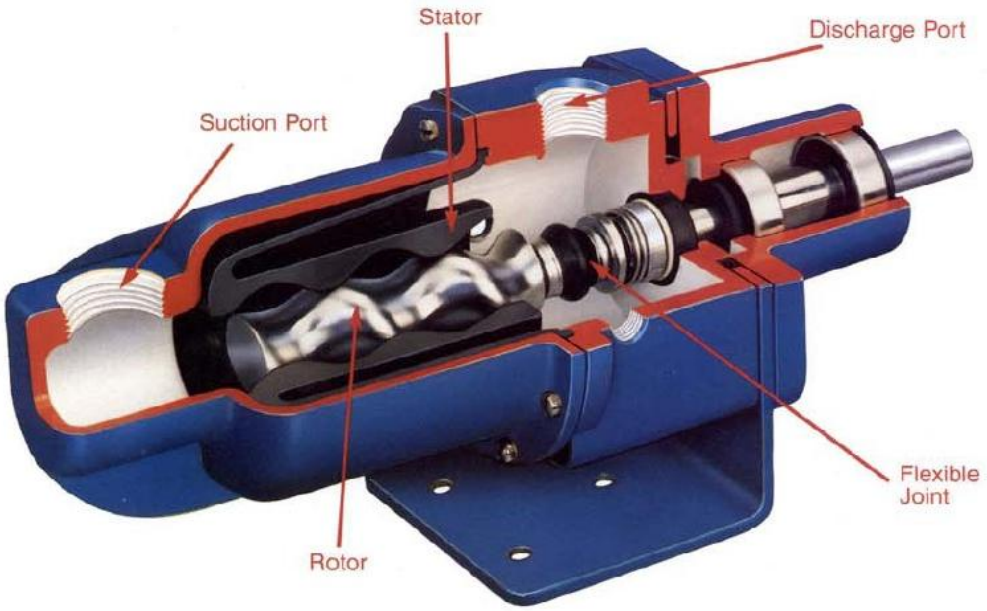

Figure 6: Moyno® 500 series progressive cavity pump [32]

3.1.4 Flowmeter

The flowmeter, like the pump, was the same one used in the upstream experiment. To avoid direct mechanical contact between the flowmeter and MPCM particles, a non-intrusive electromagnetic flowmeter was used. The flowmeter is an Omega® FMG 400 1/2" ID electromagnetic flowmeter. The accuracy is ± 0.25% full scale or ±0.5% of rate at <1.0 m/s. It

can operate up to temperatures of 120°C and pressures of 2000 kPa (290 PSI). A picture of the style of flowmeter can be seen in Figure 7 which was connected to the data acquisition system. The flowrate for each test was recorded using a computer.

Figure 7: Omega® FMG 400 series flowmeter [33]

3.1.5 Water Chiller

The shell side water was cooled and pumped by an air-cooled water chiller. The chiller used was a Shini USA BWA AC-5. It consists of one 3.7 kW (5 HP) compressor with a nominal capacity of 4.8 tons. The water pump is a 0.746 kW (1 HP), centrifugal, multi-stage pump with a nominal flowrate of 0.76 l/sec (12 GPM). This style of chiller can be seen in Figure 8. The shell side flowrate was recorded for each test off of the readout on the outside of the water chiller.

Figure 8: Shini USA air-cooled water chiller [34]

3.1.6 Thermocouples

The thermocouples used were Type-T immersion thermocouples. The thermocouples were placed in a PVC Tee housing, in-line with the individual inlet and outlet flows.

3.1.7 Data Acquisition

The temperature data used in this experiment was taken using a data acquisition system. An Agilent 34970A Data Acquisition Unit was used with the Agilent Benchlink Data Logger software. The data acquisition system can measure up to 11 different input signals including temperatures from thermocouples, DC and AC voltages and currents, as well as frequency and periods. The unit has a built in digital multi-meter with a six and a half digits of resolution. The system is reported as having 0.004% basic DC V accuracy. The unit has USB flash drive data logging capability. The system allows for per channel configurability in order to measure different ranges on each channel. The Agilent software uses a graphical user interface to display and analyze the results in real time. A schematic of the entire experiment can be seen in Figure 9.

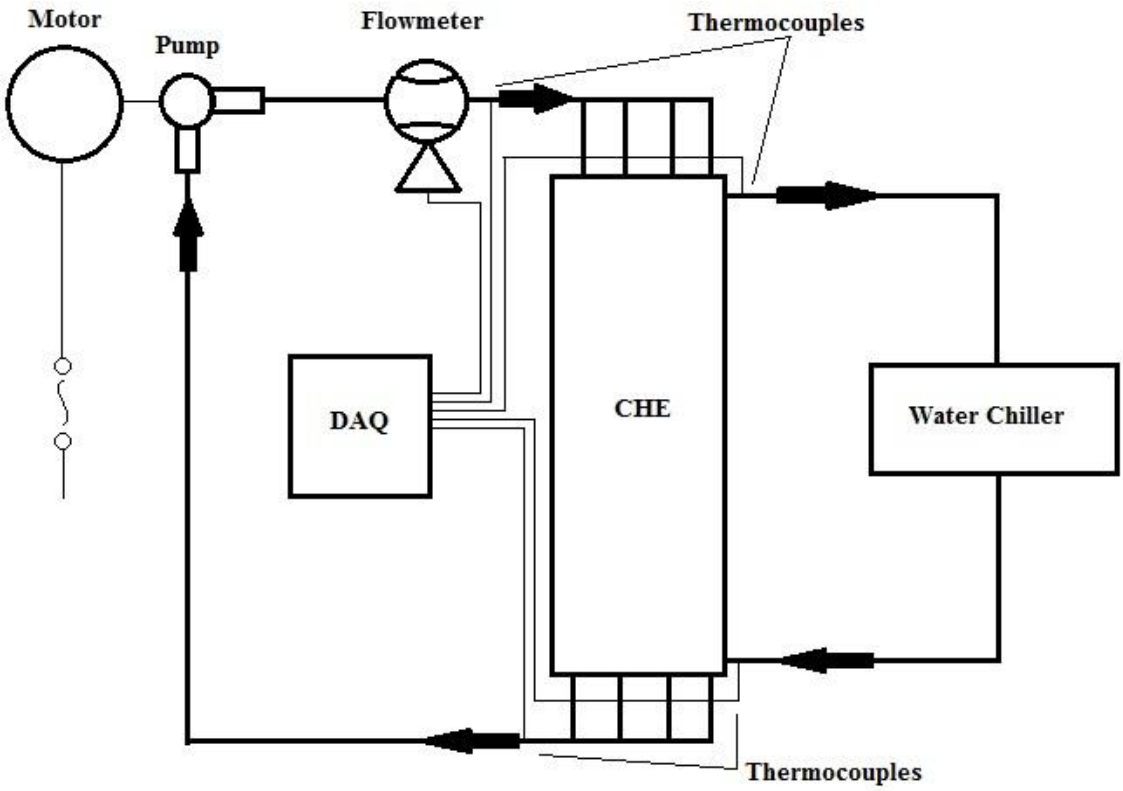

Figure 9: Schematic of the heat transfer experiment

3.2 Data Reduction

During the experiments, temperatures for the inlet and outlet of the coil and shell side heat exchanger as well as flowrates were acquired. In order to analyze these data in a meaningful manner, an extensive amount of data reduction has been generated.

3.2.1 Fluid Properties

The fluid properties on the shell and coil sides were consistently evaluated at the mean temperature of their respective inlet and outlet temperatures, as seen in Equation (35).

$$T_m = \frac{T_i + T_o}{2} \tag{35}$$

The fluid properties of water were evaluated from the NIST Theromphysical Property Database for water at 1 Atmosphere [35]. The MPCMs were made using methyl stearate as the PCM and a pulyurea/polyurethane mixture as the encapsulating material. The MPCMs were seen to have particle sizes less than 7 μm. For the fluid properties of the MPCM slurry, due to the complex nature of the slurry, different methods were used to calculate its properties. The viscosity of the slurry was measured using a rotary viscometer at three different shear rates as seen in Figure 10. A linear curve fit to the data was used to approximate the viscosity over the whole experimental temperature range.

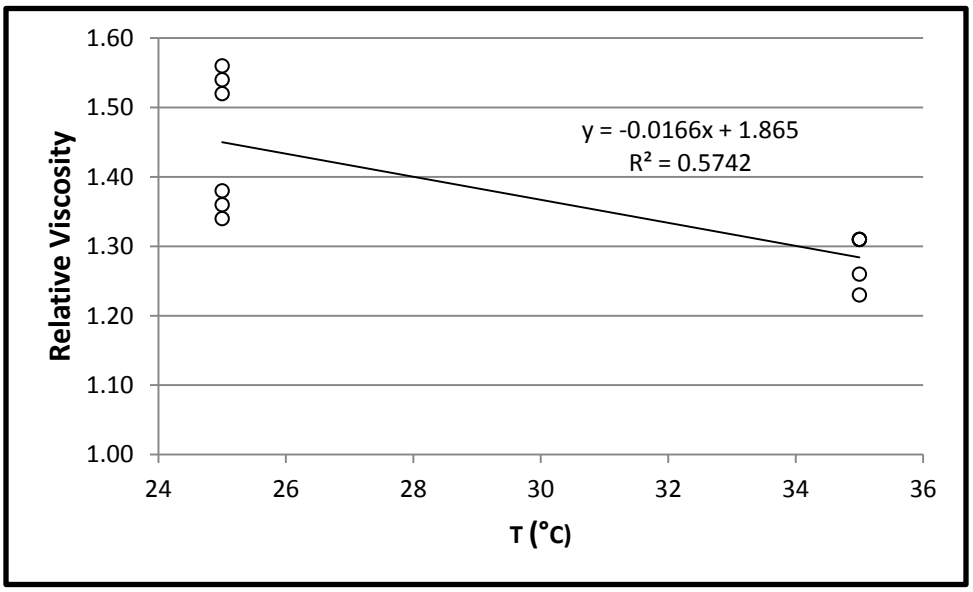

Figure 10: MPCM slurry experimental viscosity data

The density of the MPCM particles was measured previously by Tumuluri under the guidance of Dr. Alvarado and is taken as an average of 868 kg/m^3 over the temperature range. The density of the MPCM slurry was calculated using Equation (36), based upon mass fraction and density of the MPCM.

$$\rho_{slurry} = \frac{1}{\frac{c_m}{\rho_{MPCM}} + \frac{1 - c_m}{\rho_w}} \tag{36}$$

In order to account for the large increase in c_p during melting, an effective specific heat model, seen in Equation (37), was introduced by Mulligan (1996), which takes into account the portion of the fluid that underwent phase change. The sensible heat capacity of the MPCM particle was calculated using the correlation developed by Bommel et al. [36] as seen in Equation (38). The correlation is dependent upon absolute temperature and *n*, the number of carbon atoms in the parent carboxylic acid minus one. In the present case of methyl stearate ($CH_3(CH_2)_{16}COOCH_3$), also known as methyl octadecanoate, the parent acid is stearic acid ($CH_3(CH_2)_{16}COOH$), also known as octadecanoic acid, which has 18 carbon atoms. For proper unit conversion, the molar mass of methyl stearate was calculated to be 298.51 g/mol.

$$C_{p,eff} = c_m C_{p,MPCM} + (1 - c_m) C_{p,w} + \frac{c_m \lambda}{\Delta T} \tag{37}$$

$$C_p(n, T) = \{103.16 + 16.273n + 0.04735n(T/\mathrm{K})\} \ [\mathrm{J \cdot K \cdot mol^{-1}}] \tag{38}$$

The latent heat of fusion of the MPCM was studied previously and measured experimentally. Due to the microencapsulation, the onset temperature of melting and solidification while undergoing heating or cooling changes. There is also some variation in the latent heat of melting and fusion during this process. Experimental differential scanning calorimetry (DSC) data of the MPCMs taken previously under the guidance of Dr. Alvarado showed a latent heat of fusion while undergoing cooling to be 171.3 kJ/kg.

The thermal conductivity of the MPCM is calculated using a curve fit based upon previous research. The curve fit is valid over the coil side temperature range and is seen in Equation (39). The MPCM slurry thermal conductivity was calculated using Maxwell's equation for predicting conductivity of two-phase mixtures [37] as seen in Equation (40).

$$k_{MPCM} = -0.0002 \cdot T_{H,Avg} + 0.2012 \tag{39}$$

$$k_{slurry} = k_w \frac{2k_w + k_{MPCM} - 2F_{MPCM}(k_w - k_{MPCM})}{2k_w + k_{MPCM} + F_{MPCM}(k_w - k_{MPCM})} \quad (40)$$

In order to study the effectiveness of using MPCMs in a CHE, we must analyze the raw data using the Log Mean Temperature Difference (LMTD) method as well as the Effectiveness versus NTU (ε-NTU) method for heat exchangers.

3.2.2 Log Mean Temperature Difference

Due to the non-linear nature of the fluids' temperature change in a heat exchanger caused by the phase change process, the average temperature difference, ΔT_m, varies with axial distance. A differential element approach was needed to determine the form of ΔT_m. In Equation (41) and (42), we apply an energy balance to the differential elements of the coil and shell side fluids. In the case of the present experiment, the coil side contains the hotter of the two fluids. C_h and C_c in this case are the heat capacity rates of the respective fluids. The differential heat transfer can also be calculated based upon a differential surface area, dA, using Equation (43) where ΔT is the local temperature difference calculated as $\Delta T = T_h - T_c$.

$$dq = -\dot{m}_h C_{p,h} dT_h = -C_h dT_h \quad (41)$$

$$dq = -\dot{m}_c C_{p,c} dT_c = C_c dT_c \quad (42)$$

$$dq = U\, \Delta T\, dA \quad (43)$$

If we substitute Equations (41) and (42) into the local differential temperature difference in Equation (44) we obtain Equation (45). Substituting this equation into Equation (43), we arrive at Equation (46), which can be integrated over the length of the heat exchanger.

$$d(\Delta T) = dT_h - dT_c \tag{44}$$

$$d(\Delta T) = -dq\left(\frac{1}{C_h} + \frac{1}{C_c}\right) \tag{45}$$

$$\int_1^2 \frac{d(\Delta T)}{\Delta T} = -U\left(\frac{1}{C_h} + \frac{1}{C_c}\right)\int_1^2 dA \tag{46}$$

$$\ln\left(\frac{\Delta T_2}{\Delta T_1}\right) = -\frac{UA}{q}(\Delta T_2 - \Delta T_1) \tag{47}$$

For a counter-flow heat exchanger:

$$\Delta T_1 = T_{h,i} - T_{c,o}$$
$$\Delta T_2 = T_{h,o} - T_{c,i}$$

Rearranging (47):

$$q = UA\frac{\Delta T_2 - \Delta T_1}{\ln\left(\frac{\Delta T_2}{\Delta T_1}\right)} \tag{48}$$

Evaluating the integral and substituting the non-differential forms of Equations (41) and (42) for C_h and C_c we arrive at Equation (47) and its more prevalent form seen in Equation (48). As this equation is the non-differential form of Equation (43), we can see the correct temperature difference for heat exchanger analysis is the log mean temperature difference (LMTD) as seen in Equation (49). This process is covered in detail by Incropera [1].

$$\Delta T_{lm}\frac{\Delta T_2 - \Delta T_1}{\ln\left(\frac{\Delta T_2}{\Delta T_1}\right)} \tag{49}$$

3.2.3 Heat Transfer Formulation

The total amount of heat transfer in the system can be calculated from either the coil side or the shell side. Due to all tests having water as the working fluid on the shell side, the shell side heat transfer rate was calculated using Equation (50) for further analysis. The heat transfer rate can be used in conjunction with the LMTD method in order to calculate the overall heat transfer coefficient, *U*, as seen in Equation (51) and in its resistance network form in Equation (52). A diagram of the resistance network can be seen in Figure 11. In this network, the conduction through the coil tube has been neglected.

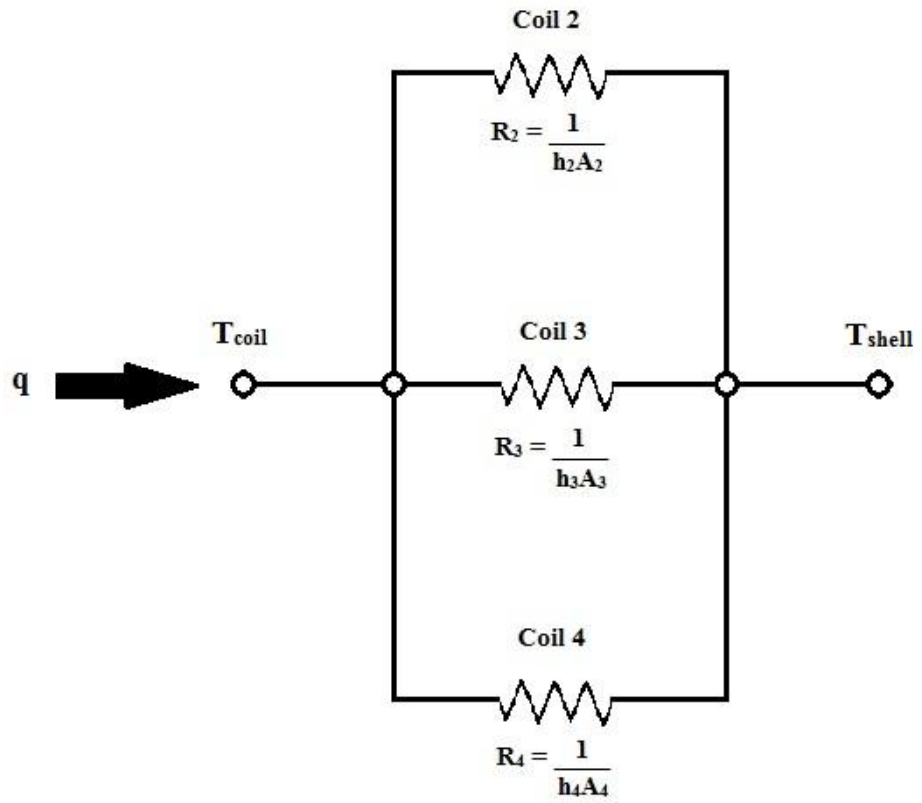

Figure 11: Resistance network diagram of the CHE

$$q = \dot{m}_s C_{p,w}\left(T_{s,o} - T_{s,i}\right) \tag{50}$$

$$q = U_i A_i \Delta T_{lm} = U_o A_o \Delta T_{lm} \tag{51}$$

$$\frac{1}{UA} = \frac{1}{U_i A_i} = \frac{1}{U_o A_o} \tag{52}$$
$$\frac{1}{UA} = \frac{1}{h_i A_i} + \frac{1}{h_o A_o}$$

Using the overall heat transfer coefficient calculated from Equation (51), the only unknowns in Equation (52) are the shell and coil side heat transfer coefficients. To determine the shell side heat transfer coefficient, tests with water flowing through the shell and coil sides were run first. An inner heat transfer coefficient for the coil side was calculated from a proven coil heat transfer correlation, seen in Equation (26) [19]. Calculation of shell side heat transfer coefficients were conducted for different experimental conditions.

Since each coil had different lengths and all the coils were connected in parallel, the velocity through each coil was not assumed to be the same. Under the assumption of incompressible flow, the pressure drop across each coil is given by Equation (53) which is used for coils connected in parallel. The fluid velocity in each coil varied depending on the total coil mass flowrate as predicted by Equation (54). Fluid velocities in coils 2 and 3 can be expressed in terms of coil 4's velocity, producing a set of 3 equations and 4 unknowns. To find each fluid velocity, initially a guess is given for each friction factor to calculate coil velocities and the corresponding Reynolds numbers. These Reynolds numbers are then used to calculate a friction factor based upon friction factor correlations of coiled tubes as proposed by White [38] and Ito [9] for the laminar and turbulent regimes, respectively. These correlations are presented in Equation (55) and (56). Ito [9] proposed Equation (57) as the critical Reynolds number for transition from laminar to turbulent flow. The predicted values of the friction factors are then used as the new guess in the next iteration. This process was continued until two consecutive friction factor values in each coil converged to a single value. Moreover, the Reynolds numbers for all tests were seen to be below the critical Reynolds value and were assumed to be in the laminar regime for helical tube flow. Thus, White's friction factor correlation was used in all calculations.

$$\Delta P = f_2 \rho \frac{L_2}{d} \frac{{V_2}^2}{2} = f_3 \rho \frac{L_3}{d} \frac{{V_3}^2}{2} = f_4 \rho \frac{L_4}{d} \frac{{V_4}^2}{2} \tag{53}$$

$$\dot{m} = \rho \dot{V} A_{total} = \rho \left(\dot{V}_2 A_2 + \dot{V}_3 A_2 + \dot{V}_4 A_4 \right) \tag{54}$$

$$\frac{f}{f_s} = \left\{ 1 - \left[1 - \left(\frac{11.6}{De} \right)^{0.45} \right]^{2.22} \right\}^{-1} \tag{55}$$

Valid for: $11.6 < De < 2{,}000$

$$\frac{f}{f_s} = \left[Re \left(\frac{d}{D} \right)^2 \right]^{1/20} \tag{56}$$

Valid for: $6{,}000 < Re < 65{,}000$

$$Re_{cr} = 2 \times 10^4 \left(\frac{d}{D} \right)^{0.32} \tag{57}$$

Using Reynolds number and the corresponding Dean number, the Nusselt number correlation proposed by Salimpour [19], seen in Equation (26), was chosen based upon its similar design and operational parameters including coil to tube diameter ratios, pitch, and Prandtl number. A comparison of these parameters can be seen in Table 2. The correlation proposed by Salimpour [19] was chosen since it provides the best fit to the present experiments including the use of water in the coils, similar heat exchanger boundary condition, as well as its Dean number range of 1000-5000. Since the correlation is only valid for individual coils, a composite Nusselt number was calculated based upon a parallel resistance network (Figure 11) using the three coils as seen in Equation (58).

Table 2: Parameter comparison between present experiment and correlation experiment

Parameter	Present Experiment	Salimpour (2009) [19]
d	6.35 mm	9, 12 mm
D	42, 71, 100 mm	120 mm
Pitch, b	9.5 mm	17, 21.4, 267. mm
γ	0.0426 - 0.101	0.0451 - 0.0708
Tube side flowrate	0.049 - 0.090 kg/s	0.016 - 0.113 kg/s
De	918 - 3345	1000 - 5000
Pr	5.5	7

$$Nu_c = \frac{h_i d}{k} = \frac{Nu_2 A_2 + Nu_3 A_3 + Nu_4 A_4}{A_{total}} \tag{58}$$

Once inner heat transfer coefficients were calculated, the outer heat transfer coefficient for the shell side was determined when water was used as HTF in the coils and shell. A new correlation was developed and postulated based upon the present experimental data and the calculated outer heat transfer coefficient. This correlation is only valid in the range of shell side flowrates and corresponding Reynolds number range used in the experiments. The correlation, shown in Equation (59), is based upon the same form as the Dittus-Boelter correlation as was seen in Equation (1), using *n = 0.4* for heating and a hydraulic diameter based upon a projected cross section as seen in Figure 12.

$$Nu_o = 0.0461 {Re_o}^{0.8} Pr^{0.4} \tag{59}$$

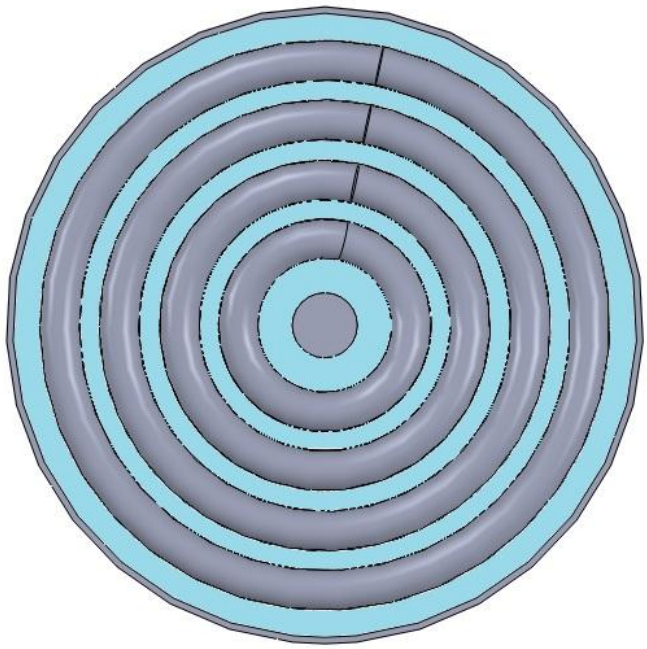

Figure 12: Projected cross section of heat exchanger, blue areas designate flow cross-section

As indicated, the shell side correlation was developed using water as the HTF both in the coils and shell sides. Once the shell side correlation was developed, it was used to study the effects of using MPCM slurry in the coils for similar flowrates. Moreover, the experimental shell side heat transfer correlation was used to calculate coil side heat transfer coefficients when MPCM slurries passed through them. The only unknown during the MPCM slurry test that could not be determined directly was the inner heat transfer coefficient, which was calculated by solving for it using Equation (50).

3.2.4 Heat Exchanger Effectiveness

The effectiveness-NTU method (ε-NTU method) has been widely used in heat exchanger analysis. The equation for effectiveness of a heat exchanger can be seen in Equation (60). The maximum heat transfer in a counterflow heat exchanger occurs when one of the fluids

experiences the maximum possible ΔT. The HTF with the smaller heat capacity rate, C (W/°C), defined in Equation (61), will reach this maximum temperature difference first. In the present study, the coil side always pertains to the fluid with the minimum heat capacity rate, C_{min}. It follows that for q_{max}, the maximum temperature difference for a counterflow heat exchanger is $T_{h,i} - T_{c,i}$. The calculated effectiveness is often used with the number of transfer units (NTU) of a heat exchanger to compare relative effectiveness of different heat exchangers. The NTU is a dimensionless number that is calculated using the overall heat transfer coefficient and the minimum heat capacity rate as seen in Equation (62) [1]. Different heat exchangers have different ε-NTU relationships and are often compared to determine the most effective heat exchanger.

$$\varepsilon = \frac{q}{q_{max}} = \frac{C_{shell}\left(T_{c,o} - T_{c,i}\right)}{C_{min}\left(T_{h,i} - T_{c,i}\right)} \tag{60}$$

$$C = \dot{m}C_p \tag{61}$$

$$NTU = \frac{UA}{C_{min}} \tag{62}$$

3.3 Results and Discussion

A helical coil heat exchanger (CHE) was built and tested using water flowing through the shell with water flowing through the coils initially. Once enough data was obtained to characterize the shell side of the CHE, an appropriate correlation for the shell side was developed and postulated as described in detail above. The developed shell side correlation was used to interpret the effects of using MPCM slurry in the coils. Inlet and outlet temperatures of the shell and coil side were measured as well as flowrates. For each individual run, coil and shell side flowrates and inlet and outlet temperatures were measured. In order to fully analyze all of the data, the tests using water in both the coils and the shell are covered first.

3.3.1 Water in Shell and Water in Coils Tests

For the case of when water in the shell and water in the coils was used, there were a total of 10 runs with three different coil side flowrates and two different shell side flowrates. The raw data for these runs can be seen in Table 3. The total calculated heat load varied from 4.5 - 6.3 kW. Proper energy balance calculations were undertaken and only an average of 5.9% discrepancy between the shell side and coil side were identified. In fact, the shell side always showed an average 5.9% higher heat loads that the coil side indicating that small heat losses between the shell side and the environment were taking place.

Table 3: Flowrates and temperature data for the case of water in shell with water in the coils

Test Number	**Tube Side Flowrate (L/s)**	**Shell Side Flowrate (L/s)**	**T_H_in (°C)**	**T_H_out (°C)**	**T_C_in °C)**	**T_C_out (°C)**
1	0.05	0.90	42.60	20.27	18.84	20.14
2	0.05	1.24	42.28	20.16	18.73	19.68
3	0.07	0.90	39.53	21.38	18.86	20.29
4	0.07	0.94	41.81	21.57	18.83	20.37
5	0.07	1.24	41.22	20.94	18.75	19.96
6	0.07	1.24	38.93	20.75	18.81	19.89
7	0.09	0.92	37.61	22.01	18.84	20.39
8	0.09	0.93	35.70	21.68	18.84	20.24
9	0.09	1.24	35.13	21.06	18.77	19.88
10	0.09	1.24	37.04	21.33	18.80	20.01

One of the objectives of the project was to quantify the heat exchanger effectiveness of the devised CHE. For that purpose, inlet and outlet temperatures as well as heat transfer rates were measured and calculated to determine effectiveness using the ε-NTU method. However, to be able to use the ε-NTU method, the overall heat transfer coefficient for the whole CHE had to be determined first when water was flowing through the coil and shell sides. Therefore, the shell

side heat transfer coefficient and Nusselt number were calculated as explained above using the data shown in Table 2.

Figure 13 depicts the composite water-based inner Nusselt number for all the coils versus average Dean number of the three coils. The three coils have a large Dean number variation but it clearly shows that as De number increases, Nusselt number increases as seen in several Dean number based correlations including the one proposed by Salimpour in Equation (26) [19]. As seen in Figure 13, the three groups of data correspond with the three different coil flowrates used. Based upon the individual coil Nusselt numbers and their different surface areas, it can be seen that coils 2, 3, and 4 have a percent contribution, *w*, to the composite Nusselt number by 47, 33, and 20 percent, respectively giving a wide range of data for a single flowrate on the shell side. This large variation is due to the difference in surface area and fluid velocity in each coil. Nevertheless, Figure 13 shows that when using more than one coil, greater rates of heat transfer can be achieved at higher Dean number making the overall heat transfer process more efficient as discussed below. An uncertainty propagation analysis was undertaken for the composite coil Nusselt number, heat exchanger effectiveness, and the number of transfer units. These uncertainties can be seen in Table A- 2 in APPENDIX A

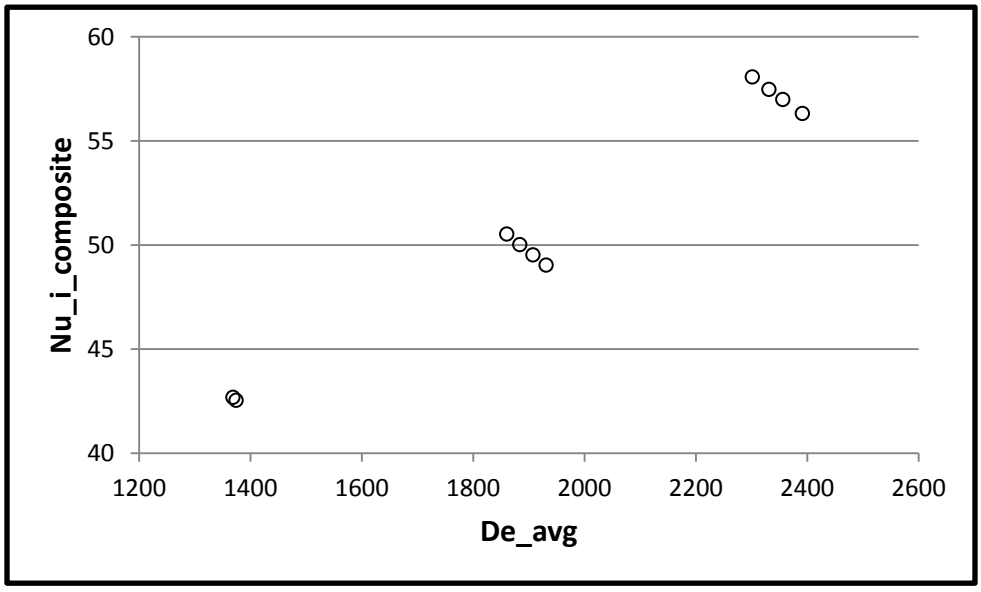

Figure 13: Composite coil Nusselt number versus average coil Dean number

Using the water-based inner Nusselt number data, shell side heat transfer coefficients and outer Nusselt numbers were calculated and can be seen in Figure 14. For ease of viewing, data points with the same coil side flowrate have the same symbol shape in the legend. As seen in the figure, at lower shell side flowrates, there is little discrepancy in Nusselt number regardless of coil side flowrate, which is to be expected. Theoretically this should also occur at the higher shell side flowrate of 1.24 L/s (19.6 GPM) but it does not. Looking further, it can be seen that for the coil side flowrates of 0.07 and 0.09 L/s, the outer Nusselt number increases with increasing shell side flowrate, but it does not for the lowest coil side flowrate of 0.05 L/s and in fact is almost the same at both shell side flowrates. The main difference in Nusselt number between low and high flow rates on the shell side can be attributed to Reynolds number in the laminar regime. At lower Reynolds number, there is less fluid separation and fluid mixing on the shell side which results in Nusselt number values more or less independent and insensitive of the conditions inside the coils; however, at higher Reynolds number in the shell, a greater degree of flow separation and fluid mixing are expected to take place which makes the shell side heat transfer coefficient (and overall heat transfer coefficient U) more dependent and sensitive on coil flow conditions. This discrepancy can also be explained if we look at the effectiveness versus NTU relationship of the heat exchanger generated using the data shown in Table 3 as seen in Figure 15. In Figure 15, effectiveness increases with increasing NTU, decreasing coil side flowrate, and increasing shell side flowrate. For the coil flowrates of 0.07 and 0.09 L/s, effectiveness increases with increasing shell side flowrate but does not for 0.05 L/s coil side flowrate. This is due to the effectiveness reaching the asymptotic limit of one, or 100% effectiveness at low coil side flowrate (limiting case) relative to the shell side flowrate. In other words, the overall heat transfer rate is dominated by shell flow conditions and no further increase in heat transfer can be obtained as long as the coil flow rate remains low, further indicating that shell side Reynolds number plays a decisive role in the overall heat transfer process. Included for reference on Figure 15 is the explicit ε-NTU relation for all heat exchangers when $C_{min}/C_{max} = 0$ as seen in Equation (63) [1].

$$NTU = -\ln(1-\varepsilon) \tag{63}$$

The present data slightly over predicts this relationship due to the as mentioned overestimation of the shell side calculated total heat rate compared to the coil side calculated total heat rate. Correspondingly, the effectiveness seen for the 0.05 L/s coil side and 1.24 L/s(19.6 GPM) shell

side flowrates is 1.06, which is physically impossible, but within 10% of the maximum theoretical value.

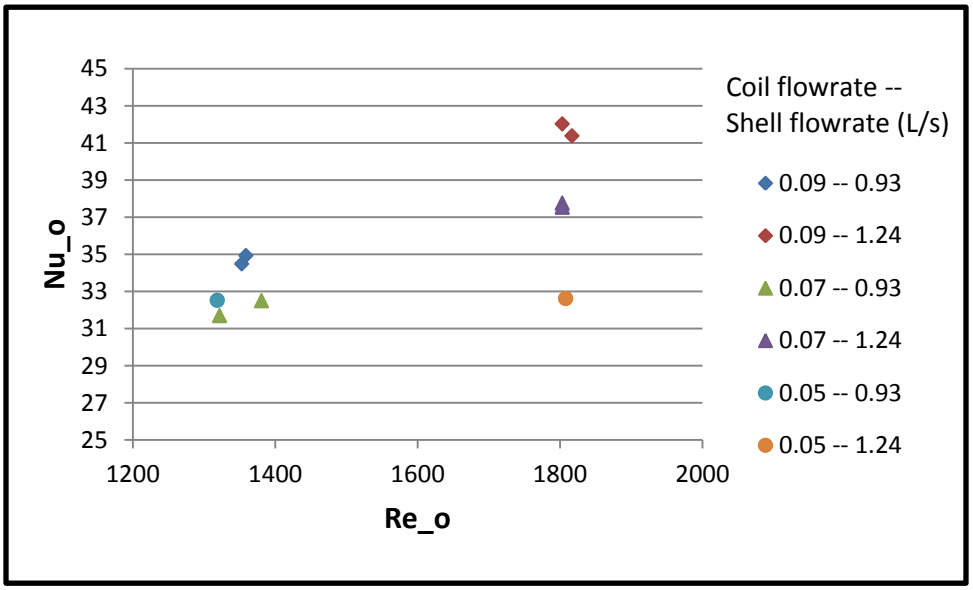

Figure 14: Shell side calculated Nusselt number versus Reynolds number

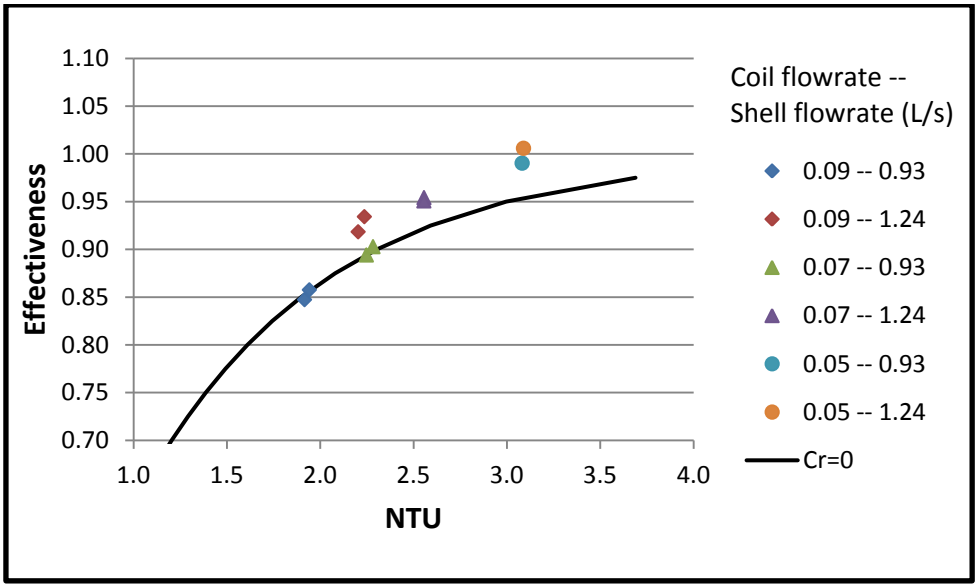

Figure 15: Effectiveness versus NTU for helical coil heat exchanger for water

In order to calculate an accurate correlation for the shell side heat transfer, we need to look at only the data points for which the amount of heat transfer is changing relative to coil and shell side flowrates. Because of this, the data point with 0.05 L/s coil side and 1.24 L/s (19.6 GPM) shell side flowrates is omitted during the calculation of the shell side heat transfer correlation. The shell side heat transfer correlation was calculated based upon a curve fit as seen in Figure 16 and presented in Equation (64). Though the correlation coefficient is 0.71, the correlation should be valid for the present experimental data set in the range of coil and shell side flowrates used. A sensitivity analysis was undertaken to see the effect of varying the coil Nusselt number on the shell side Nusselt number. This analysis can be seen in Figure A- 1 in APPENDIX A.

$$Nu_o = 0.0461 {Re_o}^{0.8} Pr^{0.4} \tag{64}$$

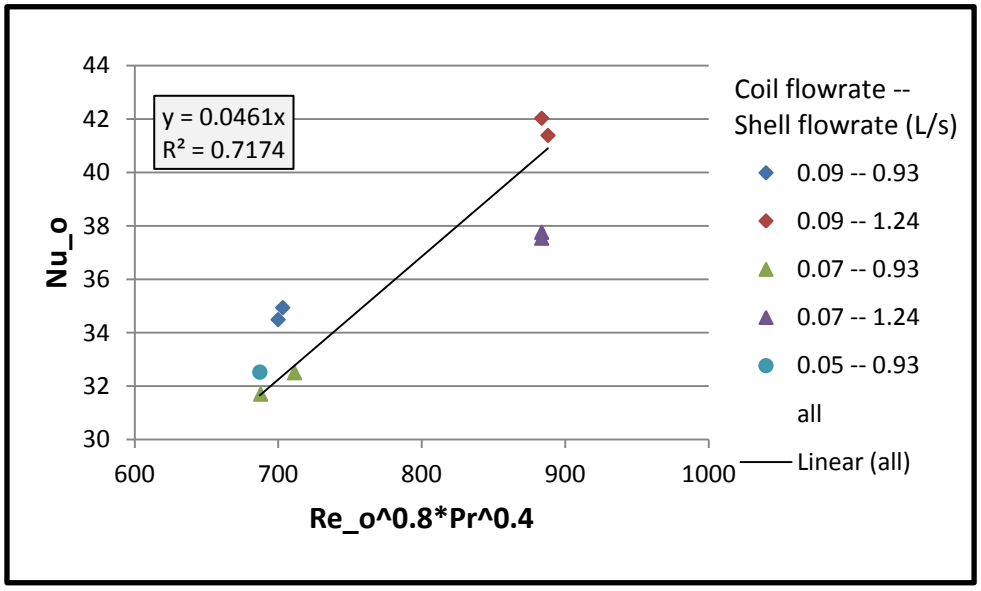

Figure 16: Curve fit for shell side Nusselt number correlation

3.3.2 Water in Shell and MPCM's in Coils Tests

The second part of the experimental plan involves using water in the shell and MPCM slurry in the coils to assess the effectiveness of the CHE when MPCMs are used. A total of 12 runs were conducted including two shell side and four coil side flowrates. The volumetric flowrates were similar to that in the first part of the experimental plan. The as-recorded data can be seen in Table 4. It can be seen that the inlet and outlet temperatures were very similar to the water-to-water case. This temperature range was chosen for the hot side to ensure complete solidification of the phase change material inside each microcapsule. Previous research under the guidance of Dr. Alvarado showed an onset of solidification of methyl stearate at 29.2 °C. As the outlet temperature of the MPCM slurry is on average 7 °C colder than this, complete solidification of the MPCM particles was always assumed.

Table 4: Flowrates and temperature data for the case of water in shell with MPCM slurry in the coils

Test Number	**Tube Side Flowrate (L/s)**	**Shell Side Flowrate (L/s)**	**T_H_in (°C)**	**T_H_out (°C)**	**T_C_in (°C)**	**T_C_out (°C)**
1	0.05	1.00	47.0	21.3	18.7	20.0
2	0.05	1.00	50.8	21.7	18.9	20.3
3	0.05	1.24	46.1	20.6	18.5	19.6
4	0.05	1.25	49.9	21.2	18.8	20.0
5	0.07	0.98	42.3	21.7	18.7	20.2
6	0.07	1.24	40.4	21.2	18.8	20.0
7	0.09	0.98	37.7	22.1	18.8	20.3
8	0.09	0.97	40.2	22.3	18.8	20.4
9	0.09	0.97	38.8	22.1	18.8	20.3
10	0.09	1.25	38.2	21.4	18.8	20.0
11	0.09	1.24	39.5	21.6	18.8	20.1
12	0.11	0.98	37.0	22.8	18.8	20.4

The total heat rate calculated based upon the shell side data varies between 5.2 and 6.7 kW. The total heat rate (Equation (50)) was alternatively calculated using the coil side data along with $C_{p,eff}$. and was seen to be on average 7.9% larger than the shell side total heat rate calculations. As shown earlier, during the tests using water the shell side total heat rate was on average 5.9% larger. This discrepancy can get attributed to the unknowns associated when calculating $C_{p,eff}$ (Equation (37)). Equation (37) is calculated using the ΔT over which the MPCM underwent phase change. Since the present experiment does not allow for the measurement of temperatures along the length of the coils, the total temperature change across the coil is used for ΔT. The MPCM is undergoing phase change only during part of the length of the coil, and thus, the ΔT is larger than it should be. This introduces an unknown amount of error into $C_{p,eff}$ and any further calculations based upon it.

The calculated effectiveness versus NTU relationship for all tests conducted during this study is depicted in Figure 17. The MPCM slurry data shows a slightly different trend when compared to the explicit ε-NTU relationship and the water data shown in the previous section. This can be attributed to the uncertainties associated with the calculation of $C_{p,eff}$. It is interesting to note that the MPCM slurry is shown to have a slightly lower effectiveness and NTU than for the water data for similar coil and shell side flowrates. This can be attributed to the MPCM's higher heat transfer coefficient as well as the MPCM slurry having a higher specific heat than water. The former of these causes an increase in UA while the latter causes an increase in C_{min}. The combination of these two causes a decrease in effectiveness as well as NTU. An uncertainty propagation analysis was undertaken for the composite coil Nusselt number, heat exchanger effectiveness, and the number of transfer units. These uncertainties can be seen in Table A- 3 in APPENDIX A.

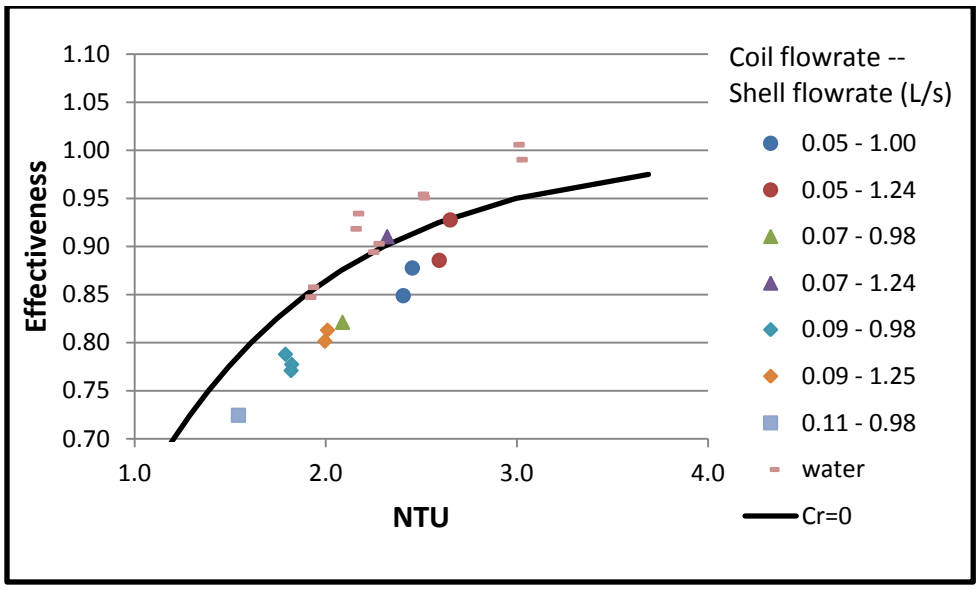

Figure 17: Effectiveness versus NTU for helical coil heat exchanger for entire study

For the shell side flow rates of interest, it can be assumed that the heat transfer in the shell acts in the same manner regardless of what fluid is inside the coils. Therefore, Equation (64) from above was used to calculate shell side heat transfer coefficients based upon Reynolds and Prandtl number ranges used. The shell side heat transfer coefficient was used in conjunction with the overall heat transfer coefficient to calculate coil side heat transfer coefficients as explained above. The calculated inner Nusselt number is the composite Nusselt number. This Nusselt number can be broken down to individual Nusselt numbers by coil using the calculated percent contribution, *w*, of each coil calculated earlier in the first part of the experiment as seen in Equation (65) for the three coils are connected in parallel.

$$A_c Nu_c = w_2 A_2 Nu_2 = w_3 A_3 Nu_3 = w_4 A_4 Nu_4 \tag{65}$$

The calculated individual coil Nusselt numbers are plotted in Figure 18-20 along with several correlations presented earlier in the literature review section. The correlations shown in the figures are only valid for single-phase fluids while the present data is based on MPCM slurry undergoing solidification. The plots show the data in terms of $Nu/Pr^{0.3}$ $vs.$ De to be able to determine the effects of phase change process on the overall heat transfer process. The value of the Prandtl number when using MPCM slurries was estimated by the use of $C_{p,eff}$ and Maxwell's

equation for thermal conductivity of a binary mixture as explained earlier which takes into account the phase change process in a rather macroscopic manner. As seen from the three figures, each coil operates in a different range of Dean numbers but with similar range of coil Nusselt number. A curve fit to the data in the form of Equation (66) was conducted by minimizing the residual sum of squares, also known as SSE, as seen in Equation (67) [19]. The exponential constant of Prandtl number was chosen as 0.3 for consistency purposes with the other correlations since the MPCM slurry also underwent cooling during all the experiments. Equation (68) is the proposed Nusselt number correlation for MPCM slurries in a multiple coil system based on common parameters including the fluid's Dean number. This correlation is also plotted in Figure 18-20 classified as 'Predicted'. We can see that the proposed correlation fits the experimental well when taking into account the chosen parameters of *De*, *Pr*, and γ. However, the developed Nusselt number correlation curve is steeper than the other correlations which can be attributed to the fact that three coils were used instead of one (most correlations only account for one coil). Moreover, MPCM slurries at low Reynolds (or Dean number) could result in a rather complicated flow structure due to the presence of microcapsules capable of inducing a micro-convective effect not seen in single phase fluids [26]. The same parameters seen in other correlations were chosen in order to produce one general correlation that covers the different operating conditions of the three coils.

$$Nu_i = C_1 De^{C_2} Pr^{0.3} \gamma^{C_3} \tag{66}$$

$$SSE(C_1, C_2, C_3) = \sum_{i=1}^{N} \{\ln(Nu_i) - [\ln C_1 + C_2 \ln De_i + 0.3 \ln Pr_i + C_4 \ln \gamma_i]\}^2 \tag{67}$$

$$Nu_i = 1.48 \times 10^{-5} De^{1.65} Pr^{0.3} \gamma^{-1.41} \tag{68}$$

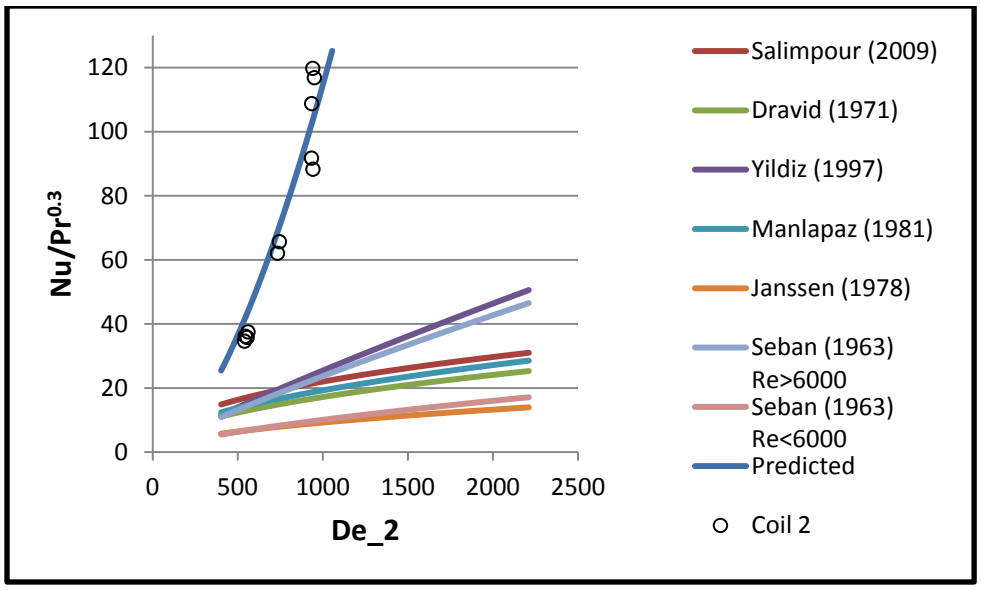

Figure 18: Calculated inner Nusselt number versus Dean number for Coil 2

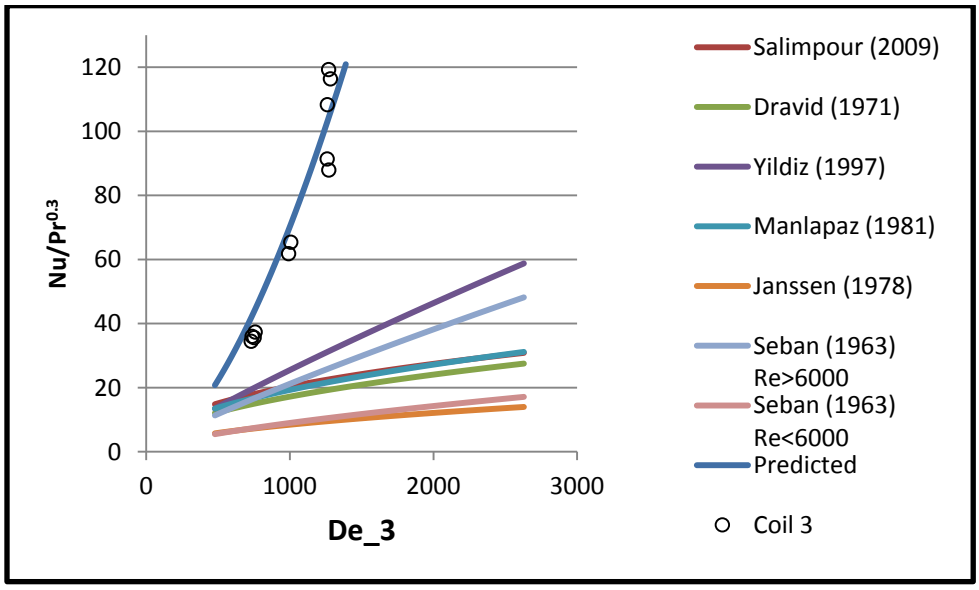

Figure 19: Calculated inner Nusselt number versus Dean number for Coil 3

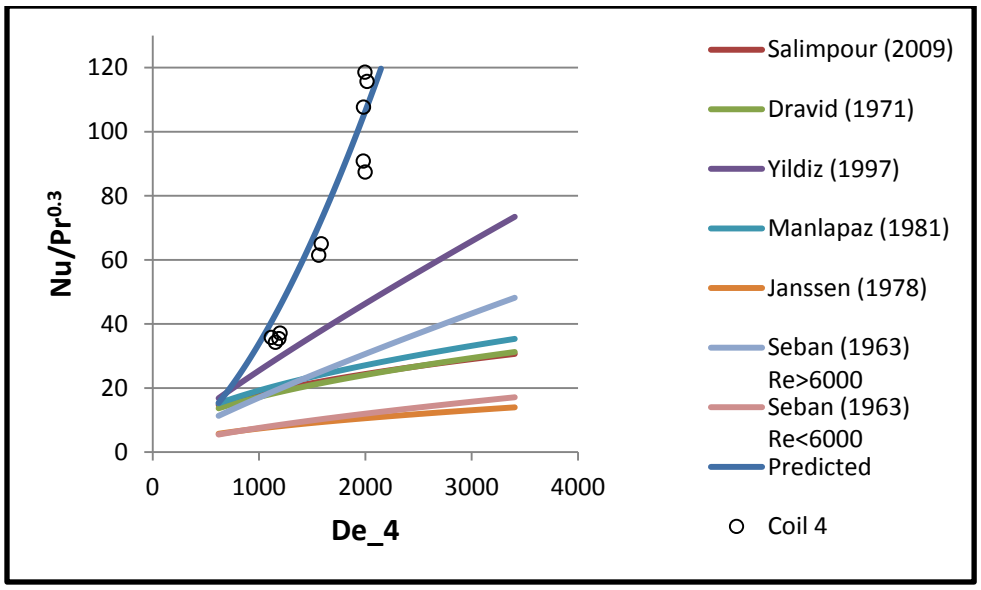

Figure 20: Calculated inner Nusselt number versus Dean number for Coil 4

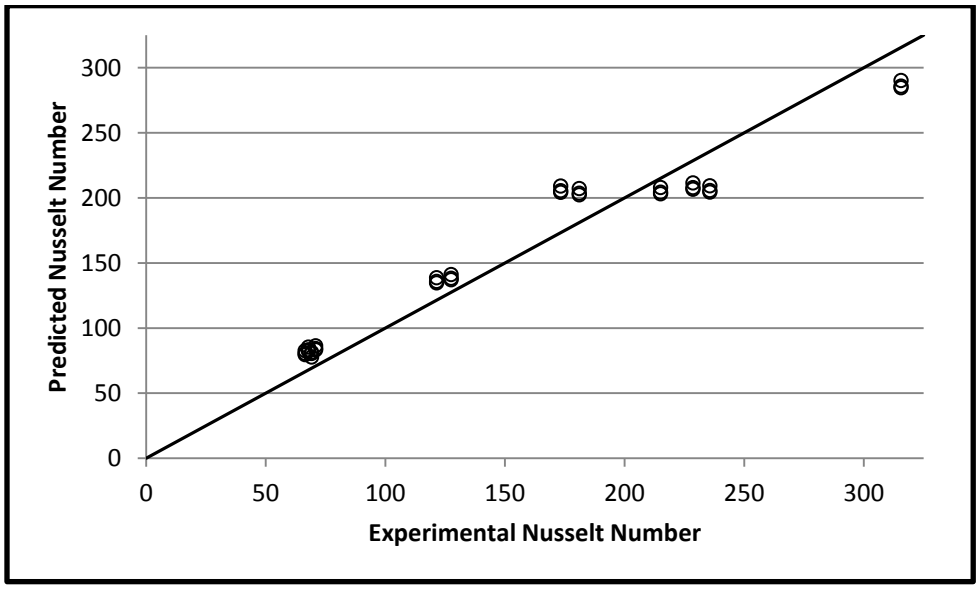

Figure 21: Comparison of Predicted versus Experimental Nusselt number for the coil side

To verify the validity of the developed Nusselt number correlation, Figure 21 shows the comparison between predicted and experimental Nusselt numbers with an average error of 14% and an R^2 correlation coefficient of 0.92. It is important to highlight that since the correlation is

exponential relative to Dean number, it should not be used outside of the range of $540 < De < 2420$.

As we can see from Figure 18-20, the Nusselt numbers for the MPCM slurry is almost always higher than what was seen in previous studies. Because the effect of the latent heat of fusion was taken into account during the calculation of the specific heat and consequently the Prandtl number, we must look to different mechanisms for this anomalous increase in heat transfer. The fluid dynamics in helical coil flow has been studied extensively using single-phase fluids, but as there are a percentage of micro particles in the fluid, the dynamics could behave differently as suggested above. In a straight pipe, the increased viscosity of MPCM slurry is seen to slow down the movement of particles from the core of the flow to the wall. A turbulent flow is needed to move the MPCM particles in the core to the wall in order to release its heat under cooling. In single-phase helical coil flow, centrifugal forces impart a lateral movement of the inner core to the outside edge of the coil possibly resulting in a cyclical process. Because of this possible circulating movement that is present even in the laminar regime, it is plausible that much more of the MPCM particles are able to interact with the wall and transfer their heat to the shell side fluid which wouldn't otherwise occur in straight tube laminar flow. Previous studies have also seen markedly different fully developed temperature profiles based upon increasing Prandtl numbers which could be another contributing factor [5].

Analysis of the results should also take into account how the proposed correlation was developed. Initially, a single correlation was chosen to represent heat transfer through the individual coils. The correlation was based off of a counter-flow heat exchanger with a single coil. The heat exchanger used in the present experiment was built quite differently, with multiple coils in close proximity to each other, all in one shell. Because of this difference, we can assume there are other possible convective heat transfer mechanisms that should be explored by conducting a thorough study with single phase fluids first. Moreover, the fact that three coils were used with different curvature diameters and different experimental Dean numbers, it suggests that plainly relying on single coil correlation provides a limited estimate of the overall heat transfer process.

Other factors that should be considered in the future include the collection of pressure drop data per coil to estimate the velocity through each coil more accurately. Currently, there is a certain level of uncertainty in the results given the number of variables involved in each experiment.

Nevertheless, the study shows that multiple coils connected in parallel provide a good way to transfer heat effectively as described above.

Another assumption made during the analysis was the use of an effective specific heat for MPCMs that takes into account the latent heat of fusion. The equation is normally used to calculate specific heats while the MPCMs are undergoing phase change. In the present case, the MPCM slurry will spend an amount of time as a multiphase fluid over an unknown length of coil, while the rest of the time it is assumed to be in the single-phase regime. Because the temperature range from the inlet and outlet of the coils covers both regimes and there is no data available to pin down when and where the phase change process occurs. Therefore, the total coil temperature difference must be used in the calculation of the effective specific heat which makes it difficult to assess the effect of phase change during the whole heat transfer process. Nevertheless, the data suggests that the devised CHE does improve the rate of heat transfer of MPCM slurries when compared to straight heat transfer sections.

4. SUMMARY AND FUTURE STUDY

The present experimental study has shown using MPCM slurry results in increased heat transfer relative to similar single-phase fluids. An initial set of tests were conducted in a multiple helical coil heat exchanger using water in the shell and water in coils in order to calculate a shell side heat transfer correlation. This correlation was then used during a second set of tests involving MPCM slurry in the coils in order to understand the effects of using MPCM slurry on heat transfer in a CHE. Increases in heat transfer seem to be largely affected by many of the assumptions required to complete the analysis. Past studies have shown that even with the increased specific heat of a MPCM slurry, its heat transfer has been shown to perform worse than water in straight tubes. On the other hand, fluids in helical coils have been shown to perform better than straight tubes. As this is the first experimental evidence of the combination of the two, the increases in heat transfer seen garner enough attention for future study.

Previous experimental studies on shell and coil heat exchangers have shown good agreement with corresponding numerical simulations. In order to more reliably study the effects of the use of MPCM slurry in helical heat exchangers, a numerical simulation of the present study is recommended. The numerical study itself would not require any of the correlations used in the present analysis and could possibly provide a more accurate understanding of the present heat exchanger. Though taking into account microparticles in the fluid can be numerically cumbersome and time consuming, the effects of phase change can be taken into account using well known heat capacity models. After this numerical analysis is complete, the results can be easily compared to the present study. Future studies should focus on heat exchangers with less complicated geometry. In order to reduce the number of variables, a heat exchanger with just one coil would allow for more reliable data. A helical coil with an operating Dean number of around 1000 to 2000 should produce comparable results. The present study as well as any future studies on helical coil heat exchangers involving MPCM slurries will help strengthen the field of fluid dynamics and heat transfer in the quest for superior heat transfer methods.

REFERENCES

[1] Incropera, F. P., and DeWitt, D. P., 2002, *Introduction to Heat Transfer*, John Wiley & Sons, New York, NY.

[2] Seban, R. A., and McLaughlin, E. F., 1963, "Heat Transfer in Tube Coils with Laminar and Turbulent Flow," International Journal of Heat and Mass Transfer, **6**(5) pp. 387-395.

[3] Dravid, A. N., Smith, K. A., Merrill, E. W., 1971, "Effect of Secondary Fluid Motion on Laminar Flow Heat Transfer in Helically Coiled Tubes," AICHE Journal, **17**(5) pp. 1114-1122.

[4] Dwane Paulsen's Blog, 2010, "Coiled-tube Heat Exchanger", from http://www.dwanepaulsen.net/blog/2009/04/coiled-tube-heat-exchanger/

[5] Kalb, C. E., and Seader, J. D., 1974, "Fully Developed Viscous-Flow Heat Transfer in Curved Circular Tubes with Uniform Wall Temperature," AICHE Journal, **20**(2) pp. 340-346.

[6] Janssen, L. A. M., and Hoogendoorn, C. J., 1978, "Laminar Convective Heat Transfer in Helical Coiled Tubes," International Journal of Heat and Mass Transfer, **21**(9) pp. 1197-1206.

[7] Manlapaz, R. L., and Churchill, S. W., 1981, "Fully Developed Laminar Convection from a Helical Coil," Chemical Engineering Communications, **9**(1-6) pp. 185-200.

[8] Prasad, B. V. S. S. S., Das, D. H., and Prabhakar, A. K., 1989, "Pressure Drop, Heat Transfer and Performance of a Helically Coiled Tubular Exchanger," Heat Recovery Systems & CHP, **9**(3) pp. 249-256.

[9] Ito, H., 1958, "Friction factors for turbulent flow in curved pipes," ASME Meeting, Anonymous American Society of Mechanical Engineers (ASME), New York, NY, United States, pp. 9.

[10] Yildiz, C., Bicer, Y., and Pehlivan, D., 1997, "Heat Transfer and Pressure Drop in a Heat Exchanger with a Helical Pipe Containing Inside Springs," Energy Conversion and Management, **38**(6) pp. 619-624.

[11] Guo, L., Chen, X., Feng, Z., 1998, "Transient Convective Heat Transfer in a Helical Coiled Tube with Pulsatile Fully Developed Turbulent Flow," International Journal of Heat and Mass Transfer, **41**(19) pp. 2867-2875.

[12] Rennie, T. J., and Raghavan, V. G. S., 2005, "Experimental Studies of a Double-Pipe Helical Heat Exchanger," Experimental Thermal and Fluid Science, **29**(8) pp. 919-924.

[13] Fernandez-Seara, J., Uhia, F. J., Sieres, J., 2007, "A General Review of the Wilson Plot Method and its Modifications to Determine Convection Coefficients in Heat Exchange Devices," Applied Thermal Engineering, **27**(17-18) pp. 2745-2757.

[14] Kumar, V., Saini, S., Sharma, M., 2006, "Pressure Drop and Heat Transfer Study in Tube-in-Tube Helical Heat Exchanger," Chemical Engineering Science, **61**(13) pp. 4403-4416.

[15] Naphon, P., 2007, "Thermal Performance and Pressure Drop of the Helical-Coil Heat Exchangers with and without Helically Crimped Fins," International Communications in Heat and Mass Transfer, **34**(3) pp. 321-330.

[16] Salimpour, M. R., 2008, "Heat Transfer Characteristics of a Temperature-Dependent-Property Fluid in Shell and Coiled Tube Heat Exchangers," International Communications in Heat and Mass Transfer, **35**(9) pp. 1190-1195.

[17] Salimpour, M. R., 2007, "Numerical and Experimental Analysis of Flow and Heat Transfer in Shell and Coiled Tube Heat Exchangers for Different Geometries and Variable-property Fluids", Ph.D. thesis, University of Tehran, Iran.

[18] Kharat, R., Bhardwaj, N., and Jha, R. S., 2009, "Development of Heat Transfer Coefficient Correlation for Concentric Helical Coil Heat Exchanger," International Journal of Thermal Sciences, **48**(12) pp. 2300-2308.

[19] Salimpour, M. R., 2009, "Heat Transfer Coefficients of Shell and Coiled Tube Heat Exchangers," Experimental Thermal and Fluid Science, **33**(2) pp. 203-207.

[20] Mandal, M. M., and Nigam, K. D. P., 2009, "Experimental Study on Pressure Drop and Heat Transfer of Turbulent Flow in Tube in Tube Helical Heat Exchanger," Industrial and Engineering Chemistry Research, **48**(20) pp. 9318-9324.

[21] Mirgolbabaei, H., Taherian, H., Domairry, G., 2010, "Numerical Estimation of Mixed Convection Heat Transfer in Vertical Helically Coiled Tube Heat Exchangers," International Journal for Numerical Methods in Fluids, **66**(7) pp. 805-819.

[22] Ghorbani, N., Taherian, H., Gorji, M., 2010, "Experimental Study of Mixed Convection Heat Transfer in Vertical Helically Coiled Tube Heat Exchangers," Experimental Thermal and Fluid Science, **34**(7) pp. 900-905.

[23] Ghorbani, N., Taherian, H., Gorji, M., 2010, "An Experimental Study of Thermal Performance of Shell-and-Coil Heat Exchangers," International Communications in Heat and Mass Transfer, **37**(7) pp. 775-781.

[24] Yamagishi, Y., Takeuchi, H., Pyatenko, A. T., 1999, "Characteristics of Microencapsulated PCM Slurry as a Heat-Transfer Fluid," AICHE Journal, **45**(4) pp. 696-707.

[25] Hu, X., and Zhang, Y., 2002, "Novel Insight and Numerical Analysis of Convective Heat Transfer Enhancement with Microencapsulated Phase Change Material Slurries: Laminar Flow in a Circular Tube with Constant Heat Flux," International Journal of Heat and Mass Transfer, **45**(15) pp. 3163-72.

[26] Alvarado, J. L., Marsh, C., Sohn, C., 2007, "Thermal Performance of Microencapsulated Phase Change Material Slurry in Turbulent Flow Under Constant Heat Flux," International Journal of Heat and Mass Transfer, **50**(9-10) pp. 1938-1952.

[27] Chen, B., Wang, X., Zeng, R., 2008, "An Experimental Study of Convective Heat Transfer with Microencapsulated Phase Change Material Suspension: Laminar Flow in a Circular Tube Under Constant Heat Flux," Experimental Thermal and Fluid Science, **32**(8) pp. 1638-1646.

[28] Zeng, R., Wang, X., Chen, B., 2009, "Heat Transfer Characteristics of Microencapsulated Phase Change Material Slurry in Laminar Flow Under Constant Heat Flux," Applied Energy, **86**(12) pp. 2661-2670.

[29] Taherian, H., and Alvarado, J. L., 2010, "System analysis of MPCM slurry enhanced with carbon nanotubes as heat transfer fluid," 2010 ASHRAE Annual Conference, June 26, 2010 - June 30, Anonymous Amer. Soc. Heating, Ref. Air-Conditoning Eng. Inc, Albuquerque, NM, United states, **116,** pp. 578-584.

[30] Nakagawa, S., Hashimoto, T., Hayashi, T., 2010, "Fundamental study on heat transfer characteristics of microencapsulated phase change material suspensions flowing in circular mini-pipe," 2010 12th IEEE Intersociety Conference on Thermal and Thermomechanical Phenomena in Electronic Systems, ITherm 2010, June 2, 2010 - June 5, Anonymous IEEE Computer Society, Las Vegas, NV, United states, .

[31] Tumuluri, K., 2010, "Thermal Performance of a Novel Heat Transfer Fluid Containing Multiwalled Carbon Nanotubes and Microencapsulated Phase Change Materials", M.S. thesis, Mechanical Engineering, Texas A&M University.

[32] Moyno, Inc, 1996, "Moyno 500 Progressive Cavity Pumps", from http://www.depcopump.com/datasheets/moyno/brochure.pdf

[33] Omega, 2011, "Electromagnetic Flowmeters", from http://www.omega.com/Green/pdf/FMG400.pdf

[34] Shini USA, "Shini USA Portable Chillers ", from http://www.shiniusa.com/dynamicdata/data/File/Shini%20USA%20Portable%20Chillers%20052311.pdf

[35] NIST, 2011, "Thermophysical Properties of Fluid Systems", from http://webbook.nist.gov/chemistry/fluid/

[36] van Bommel, M. J., Oonk, H. A. J., and van Miltenburg, J. C., 2004, "Heat Capacity Measurements of 13 Methyl Esters of n-Carboxylic Acids from Methyl Octanoate to Methyl Eicosanoate between 5 K and 350 K," Journal of Chemical & Engineering Data, **49**(4) pp. 1036-1042.

[37] Cheng, S. C., and Vachon, R. I., 1969, "The Prediction of the Thermal Conductivity of Two and Three Phase Solid Heterogeneous Mixtures," International Journal of Heat and Mass Transfer, **12**(3) pp. 249-264.

[38] White, C. M., 1929, "Streamline Flow Through Curved Pipes", Proceedings of The Royal Society A, **123**, pp. 645-663

[39] Navidi, W., 2008, *Statistics for Engineers and Scientists, Second Edition*, McGraw Hill, New York, NY.

APPENDIX A

Uncertainty Analysis

Uncertainty analysis of the experimental measurements was carried out using the Engineering Equation Solver (EES) software. The measured data which contained quantifiable uncertainties was considered to be: the dimensions of the heat exchanger, the temperature readings of the thermocouples, the mass flowrate of the coil side flowmeter, and the volume flowrate of the shell side flowmeter. The EES software follows the multivariate propagation of error formula as seen in Equation (69) [39].The uncertainties of these measured variables can be seen in Table A- 1. The uncertainty of the data acquisition system that was used in the temperature measurements was rated at 0.004% dcV and is miniscule in comparison to the magnitude of the instrument uncertainty and thus was not included in the uncertainty analysis.

If $U = U(X_1, X_2, \dots, X_n)$ with uncertainties $\sigma_1, \sigma_2, \dots, \sigma_n$, then

$$\sigma_U = \sqrt{\left(\frac{\partial U}{\partial X_1}\right)^2 {\sigma_{X_1}}^2 + \left(\frac{\partial U}{\partial X_2}\right)^2 {\sigma_{X_2}}^2 + \cdots + \left(\frac{\partial U}{\partial X_n}\right)^2 {\sigma_{X_n}}^2} \tag{69}$$

Table A- 1: Measured variables and uncertainties

Parameter	Uncertainty
d	± 0.01 mm
D	± 0.01 mm
L	± 0.01 mm
T	± 0.5 °C
$\dot{m}_{coil}$	± 0.5%
$\dot{V}_{shell}$	± 6.31x10^{-3} L/s

Uncertainties were calculated for the composite coil Nusselt number, effectiveness, and NTU for both the tests using water and MPCM slurry as the HTF. The code used in the EES program can be seen in APPENDIX B. The calculated data and their uncertainties during the water tests can be seen in Table A- 2. Nusselt number, effectiveness, and NTU data and uncertainties during the MPCM tests can be seen in Table A- 3. Due to the extensive propagation of error, large uncertainties were seen during the MPCM tests. These large uncertainties are directly tied to the relatively large uncertainty of the T Type thermocouple that were used to measure bulk temperatures. This, in combination with the small ΔT on the shell side bring some measurements and their uncertainties to equal or greater magnitudes.

Table A- 2: Calculated data uncertainties during tests using water as HTF in the coils and water in the shell

Test Number	**$Nu_{i,\ composite}$**	**Effectiveness, ε**	**NTU**
1	41.2±0.4	0.99±0.52	2.92±0.48
2	41.3±0.4	1.00±0.73	2.88±0.48
3	48.4±0.4	0.90±0.43	2.21±0.26
4	47.5±0.4	0.90±0.40	2.23±0.24
5	47.9±0.4	0.96±0.54	2.42±0.30
6	48.9±0.4	0.95±0.61	2.43±0.34
7	54.4±0.5	0.85±0.37	1.88±0.21
8	55.5±0.5	0.86±0.42	1.88±0.23
9	56.1±0.5	0.94±0.58	2.06±0.29
10	55.1±0.5	0.92±0.52	2.07±0.26

Table A- 3: Calculated data and uncertainties during tests using MPCM slurry as HTF in the coils and water in the shell

Test Number	$Nu_{i,\ composite}$	Effectiveness, ε	NTU
1	70.1±41.6	0.87±0.47	2.42±0.60
2	68.2±36.0	0.85±0.42	2.42±0.55
3	71.2±46.8	0.94±0.59	2.68±0.80
4	67.2±38.6	0.93±0.54	2.64±0.72
5	132.5±108.6	0.83±0.38	2.11±0.46
6	121.3±105.4	0.92±0.53	2.32±0.65
7	222.6±303.4	0.79±0.36	1.80±0.40
8	214.7±249.9	0.74±0.32	1.80±0.36
9	216±273.6	0.74±0.34	1.79±0.38
10	178.1±199.6	0.79±0.45	2.00±0.53
11	178.6±185.4	0.80±0.42	2.01±0.50
12	297.7±518.5	0.70±0.30	1.53±0.31

Sensitivity Analysis

A sensitivity analysis was conducted to help understand the effect of changing coil Nusselt number on the shell-side Nusselt number. This analysis can be seen in Figure A- 1.

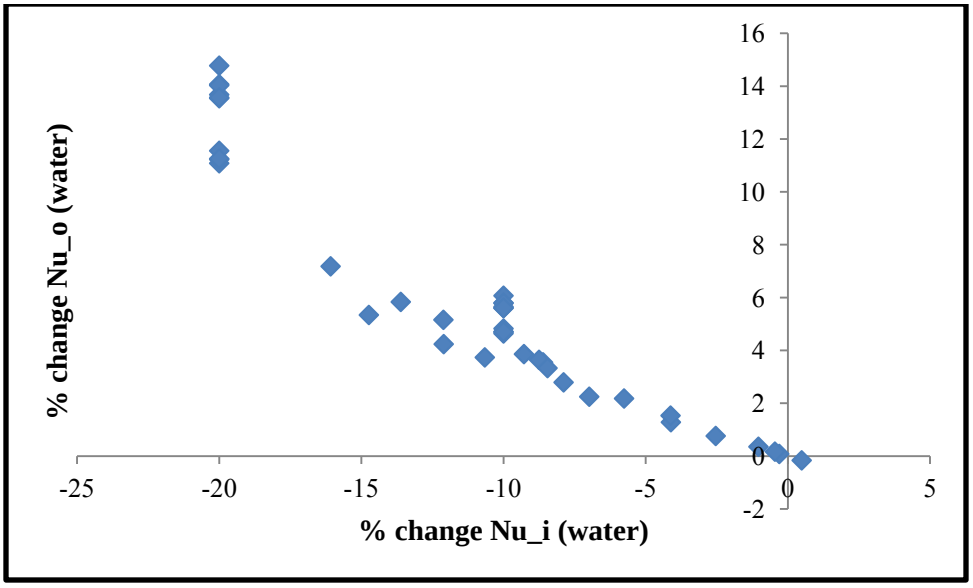

Figure A- 1: Sensitivity analysis of Nu_i on Nu_o

APPENDIX B

EES Uncertainty Analysis Code

The following code was used to perform an uncertainty analysis on the heat transfer data.

```
"Constants"
D_shell = 0.1524 [m]
OD_tube = 0.009525 [m]
ID_tube = 0.00635 [m]
D_rod = 0.015875 [m]
D_curv_1 = 0.12954 [m]
D_curv_2 = 0.100584 [m]
D_curv_3 = 0.07112 [m]
D_curv_4 = 0.042418 [m]
L_shell = 0.6096 [m]
L_coil_1 = 17.43456 [m]
L_coil_2 = 13.53312 [m]
L_coil_3 = 9.66216 [m]
L_coil_4 = 5.76072 [m]
b = 0.013462 [m]
"calculated constants"
Asurfo2 = pi*OD_tube*L_coil_2
Asurfo3 = pi*OD_tube*L_coil_3
Asurfo4 = pi*OD_tube*L_coil_4
Asurfototal = Asurfo2 + Asurfo3 +Asurfo4
Asurfi2 = pi*ID_tube*L_coil_2
Asurfi3 = pi*ID_tube*L_coil_3
Asurfi4 = pi*ID_tube*L_coil_4
Asurfitotal = Asurfi2 + Asurfi3 +Asurfi4
Acsshell = pi*D_shell^2/4
Acscoil1= pi/4*((D_curv_1+OD_tube/2)^2-(D_curv_1-OD_tube/2)^2)
Acscoil2 = pi/4*((D_curv_2+OD_tube/2)^2-(D_curv_2-OD_tube/2)^2)
Acscoil3 = pi/4*((D_curv_3+OD_tube/2)^2-(D_curv_3-OD_tube/2)^2)
Acscoil4 = pi/4*((D_curv_4+OD_tube/2)^2-(D_curv_4-OD_tube/2)^2)
Acsrod = pi*D_rod^2/4
Acsnet= Acsshell - Acscoil1 - Acscoil2 - Acscoil3 - Acscoil4 - Acsrod
Pwetshell = pi*D_shell
Pwetcoil1 = pi*(D_curv_1+OD_tube/2)+pi*(D_curv_1-OD_tube/2)
Pwetcoil2 = pi*(D_curv_2+OD_tube/2)+pi*(D_curv_2-OD_tube/2)
Pwetcoil3 = pi*(D_curv_3+OD_tube/2)+pi*(D_curv_3-OD_tube/2)
Pwetcoil4 = pi*(D_curv_4+OD_tube/2)+pi*(D_curv_4-OD_tube/2)
Pwetrod = pi*D_rod
Pwetnet = Pwetshell +Pwetcoil1 +Pwetcoil2 +Pwetcoil3 +Pwetcoil4 +Pwetrod
Dh = 4*Acsnet/Pwetnet
gamma_2 = b/(pi*D_curv_2)
gamma_3 = b/(pi*D_curv_3)
gamma_4 = b/(pi*D_curv_4)
```

```
"Measured Variables"
"using first water data as an example"
De2 = Re2*sqrt(ID_tube/D_curv_2)
De3 =  Re3*sqrt(ID_tube/D_curv_3)
De4 =  Re4*sqrt(ID_tube/D_curv_4)
C_c = rho_c*V_dot_shell*convert(l/s,m^3/s)*Cp_c
C_h = rho_h*V_dot_coils*convert(l/s,m^3/s)*Cp_h
LMTD = ((Thout - Tcin)-(Thin-Tcout))/(ln((Thout-Tcin)/(Thin-Tcout)))
Q_dot = rho_c*V_dot_shell*convert(l/s,m^3/s)*Cp_c*(Tcout-Tcin)
Q_dot_H = rho_h*V_dot_coils*convert(l/s,m^3/s)*Cp_h*(Thin-Thout)
epsilon = (C_c*(Tcout-Tcin))/(C_h*(Thin-Tcin))
u_epsilon = UncertaintyOf(epsilon)
UA = ((Q_dot_H+Q_dot)/2)/LMTD
NTU = UA/C_h
u_NTU = UncertaintyOf(NTU)
Nui2 = 0.152*De2^0.431*Pr_h^1.06*gamma_2^(-0.277)
Nui3 = 0.152*De3^0.431*Pr_h^1.06*gamma_3^(-0.277)
Nui4 = 0.152*De4^0.431*Pr_h^1.06*gamma_4^(-0.277)
Nuic = (Nui2*Asurfi2 +Nui3*Asurfi3 +Nui4*Asurfi4)/Asurfitotal
u_Nuic = UncertaintyOf(Nuic)
hi = Nuic*k_h/ID_tube
ho = (1/Asurfototal)*((1/UA)-(1/(hi*Asurfitotal)))^(-1)
Nuo = ho*Dh/k_c
u_Nuo = UncertaintyOf(Nuo)
velo = V_dot_shell*convert(l/s,m^3/s)/Acsnet
Redh = rho_c*velo*Dh/mu_c
Nuoeq = 0.0461*Redh^0.8*Pr_c^0.4
hoeq = Nuoeq*k_c/Dh
himpcm = (1/Asurfitotal)*((1/UA)-(1/(hoeq*Asurfototal)))^(-1)
Nuimpcm = himpcm*ID_tube/k_h
u_Nuimpcm = UncertaintyOf(Nuimpcm)
$Ifnot ParametricTable
mu_c = 1.0165E-03 [Pa-s]
Pr_c = 7.12004
Pr_h = 5.24395
Thin = 42.6 [C]
Thout = 20.27 [C]
Tcin = 18.84 [C]
Tcout = 20.14 [C]
V_dot_coils = 0.05 [L/s]
V_dot_shell = 0.90 [L/s]
Re2 = 3669
Re3 = 4164
Re4 = 5055
rho_c = 998.3 [kg/m^3]
rho_h = 995.220 [kg/m^3]
Cp_c = 4184.4 [j/kg-C]
Cp_h = 4184.4 [j/kg-C]
k_c = 0.59739 [W/m-C]
k_h = 0.61774 [W/m-C]
$endif
```

VITA

Travis John Gaskill received his bachelor's degree in mechanical engineering from the University of Colorado, Boulder, in 2009. His master's degree was received from Texas A&M University, College Station, in 2011. His research interests include: heat transfer and fluid flow, nanofluids, microencapsulated phase change materials, solar power and renewable energies. He plans to pursue a career in the renewable energy industry.

Mr. Gaskill can be reached at Texas A&M University Department of Mechanical Engineering, 3123 TAMU, College Station, TX 77843-3123. His email address is gaskill.travis@gmail.com.